Late Triassic high-Mg andesite/dacite suites from northern Hohxil, North Tibet: Geochronology, geochemical characteristics, petrogenetic processes and tectonic implications

Qiang Wang [a,b,*], Zheng-Xiang Li [b], Sun-Lin Chung [c], Derek A. Wyman [d], Ya-Li Sun [a], Zhen-Hua Zhao [a], Yin-Tang Zhu [e], Hua-Ning Qiu [a]

[a] State Key Laboratory of Isotope Geochemistry, Guangzhou Institute of Geochemistry, Chinese Academy of Sciences, Guangzhou 510640, PR China
[b] The Institute for Geoscience Research (TIGeR), Department of Applied Geology, Curtin University, Perth, WA 6845, Australia
[c] Department of Geosciences, National Taiwan University, P.O. Box 13-318, Taipei 10617, Taiwan
[d] School of Geosciences, The University of Sydney, NSW 2006, Australia
[e] Sedimentary Geology Institute, Chengdu University of Technology, Chengdu, 610059, China

ARTICLE INFO

ABSTRACT

This study reports age, petrologic and geochemical data for andesites and dacites from the Late Triassic sedimentary strata of northern Hohxil, in the Hohxil–Songpan–Ganzi Block (northern Tibet), which constitutes the most voluminous Triassic strata on Earth. LA-ICP-MS zircon U-Pb analysis of dacite (210.4 ± 1.9 Ma) and whole rock ^{40}Ar–^{39}Ar analyses for both the andesites and dacites (211 ± 2 Ma and 210.9 ± 1.6 Ma) show that the rocks were almost contemporaneous. Both rock types are sodium-rich and calc-alkaline. The andesites, characterized by high MgO (up to 10 wt.%) or Mg$^{\#}$ (~70), TiO$_2$, Al$_2$O$_3$, Cr, Ni, La/Yb and Th/La, but low Nb/Ta ratios, are geochemically similar to sanukitoids in southeastern Japan. The dacites are strongly peraluminous, and have high Al$_2$O$_3$ and La/Yb, low Y and Yb, coupled with negligible to positive Eu and Sr anomalies, comparable to slab-derived adakites in the circum Pacific arc system. Both rocks exhibit strongly fractionated platinum group element patterns, with Pt/Pt* (Pt anomaly), (Pt/Ir)$_N$ and Re/Os ratios higher than those of the primitive mantle. They have uniformly low εNd(t) values (-7.57–-9.59) and high ($^{86}Sr/^{87}Sr$)$_i$ ratios (0.7086–0.7106) that imply a continental rather than oceanic type magma source. We suggest that the northern Hohxil dacites were produced by partial melting of subducted sediments on the northward-subducting Songpan–Ganzi oceanic slab, and the high-Mg andesites were formed by subsequent interaction between the sediment-derived melts and mantle wedge peridotites. Taking into account the Triassic magmatic record from nearby regions, we suggest that the Late Triassic high-Mg andesite/dacite suites of northern Hohxil were generated in a forearc setting, and propose that double-sided subduction eventually closed the Songpan–Ganzi ocean during the Late Triassic.

1. Introduction

The Hohxil–Songpan–Ganzi Block (HSGB; Fig. 1a) contains the largest volume of Triassic (230–203 Ma) strata on Earth (~2.2×10^6 km^3; e.g., Nie et al., 1994), and covers >2×10^5 km^2 of the northeastern Tibetan Plateau. The source and tectonic setting of the strata, consisting of flysch or turbidite, have attracted wide interest. These sedimentary rocks were considered to have been derived by erosion of the Qinling–Dabie orogen and the North China Block to the north, the South China Block to the east, or the Qiangtang Block to the south–southwest (e.g., Bruguier et al., 1997; Nie et al., 1994; She et al., 2006; Weislogel, 2008; Weislogel et al., 2006; Yin and Harrison, 2000; Zhang et al., 2006b; Zhou and Graham, 1996). The tectonic setting of these sedimentary strata has long been disputed. Based on tectonic and sedimentary analyses, the strata were considered to have formed in a variety of tectonic settings such as an intracontinental rift (e.g., Song et al., 2004), a back-arc basin (e.g., Burchfiel et al., 1995; Pullen et al., 2008; Şengör et al., 1988; Watson et al., 1987), a foreland basin (Yuan et al., 2010), and a remnant oceanic basin (e.g., Nie et al., 1994; Weislogel, 2008; Weislogel et al., 2006; Yin and Harrison, 2000; Zhou and Graham, 1996). So far, the majority of HSGB studies have been conducted in the east, where interactions with surrounding blocks (e.g., the South China, Kunlun–Qaidam, North China, South Qinling, Qilian, Yidun, and Qiangtang Blocks; Fig. 1a) have complicated the tectonic record, possibly resulting in some of the contradicting tectonic interpretations for the sedimentary pile in the HSGB.

* Corresponding author at: State Key Laboratory of Isotope Geochemistry, Guangzhou Institute of Geochemistry, Chinese Academy of Sciences, Guangzhou 510640, PR China.
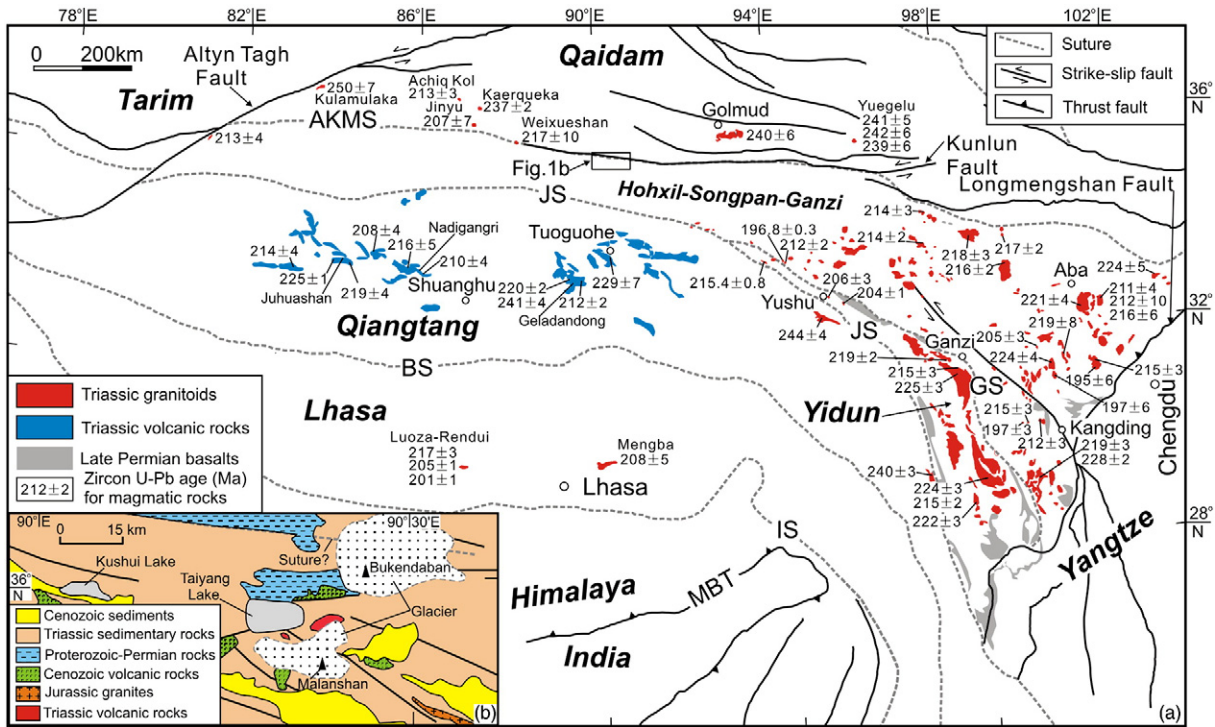E-mail address: wqiang@gig.ac.cn (Q. Wang).

Fig. 1. (a) A simplified terrane map of the Tibetan Plateau showing major crustal blocks and temporal–spatial distribution of Triassic magmatic rocks (modified from diagrams of Chung et al. (2005) and Yin and Harrison (2000)). Ages references: (Fu et al., 2010; Harris et al., 1988; Reid et al., 2007; Roger et al., 2003, 2004; Wang et al., 2008b; Weislogel, 2008; Xiao et al., 2007; Yuan et al., 2009, 2010; Zhang et al., 2006a, 2007a,b), and references therein. Main suture zones between major blocks: AKMS—Anyimaqen–Kunlun–Muztagh; JS—Jinshajiang; BS—Bangong; IS—Indus; GS—Ganzi–Litang. Major faults: MBT—Main Boundary thrust. (b) Simplified geologic map showing outcrops of magmatic rocks in the northern Hohxil area, central-western Hohxil–Songpan–Ganzi Block, northern Tibet.

Late Triassic granitoids, which mainly intrude Early–Middle Triassic and Paleozoic strata, are widespread in the eastern HSGB (Reid et al., 2007; Roger et al., 2003; Weislogel, 2008; Xiao et al., 2007; Yuan et al., 2010; Zhang et al., 2006a). These Triassic granitoids have frequently been used to constrain the tectonic setting of the Triassic strata or the subduction polarity of the HSGB or its nearby blocks (Reid et al., 2007; Roger et al., 2003; Weislogel, 2008; Xiao et al., 2007; Yuan et al., 2010; Zhang et al., 2006a). However, the granitoids mostly occur in the eastern HSGB, and contemporary magmatic rocks are scarce in the central-western part of the block (Fig. 1a). To date, even fewer Triassic volcanic rocks have been discovered in the HSGB (Qinghai, 1991; Yin and Harrison, 2000). In this study, we report the first confirmed Triassic volcanic rocks in the northern Hohxil area of central-western HSGB, near the suture between the Kunlun–Qaidam Block and HSGB (Fig. 1a and b). These volcanic rocks include high-Mg andesites that are geochemically similar to Cenozoic sanukitoids in the southeastern Japan arc (Tatsumi and Ishizaka, 1981) and dacites that are geochemically similar to Cenozoic adakites (Defant and Drummond, 1990). These distinctive rock suites help to establish the Triassic tectonic setting for the HSGB.

2. Geological setting

The Tibetan Plateau consists of a tectonic collage of different crustal blocks. From north to south, the main east–west-extending blocks are the Kunlun–Qaidam, HSGB, Qiangtang, Lhasa and Himalaya Blocks (Fig. 1a) (Chung et al., 2005; Yin and Harrison, 2000). The HSGB is a triangular tectonic unit bounded by the Anyimaqen–Kunlun–Muztagh suture to the north and the Jinshajiang (or Ganzi–Litang) suture to the south (Yin and Harrison, 2000). It is broad in the east but narrows in the west. The eastern boundary of the HSGB lies along the eastern edge of a southeast-directed, latest Triassic–Quaternary Longmenshan thrust belt on the western edge of the South China Block (Burchfiel et al., 1995). Triassic strata conformably

overlie Paleozoic shallow marine sequences of South China in the eastern HSGB, suggesting that the basement is continental, an indication of South China affinity at least in that region (Burchfiel et al., 1995; Yin and Harrison, 2000). This is consistent with the Neoproterozoic (829 ± 9 Ma) zircon U-Pb age data for granitoids in the region (Li et al., 2003; Roger and Calassou, 1997). The region has recently been interpreted as a continental peninsula that projected into the eastern Paleo-Tethys Ocean and was located along the western margin of the Yangtze Block (Zhang et al., 2006a). The HSGB extends westward through the western Kunlun Shan to Pamir (Yin and Harrison, 2000). However, no pre-Mesozoic basement rocks have so far been reported in the central-western HSGB.

Outcrops in the HSGB are commonly thick Triassic deep marine deposits (Nie et al., 1994; Qinghai, 1991; Yin and Harrison, 2000), which may have locally reached thicknesses of 10–15 km (Bruguier et al., 1997; Nie et al., 1994). The dominantly Triassic strata are commonly referred to as the Songpan–Ganzi flysch complex (Weislogel, 2008; Weislogel et al., 2006; Yin and Harrison, 2000; Zhou and Graham, 1996). Similar Triassic flysch complexes also occur to the north of the Anyimaqen–Kunlun–Muztagh suture and to the south of the Jinshajiang suture (Xiao et al., 2002a,b; Yin and Harrison, 2000). The Songpan–Ganzi flysch complex was intensely deformed by folding and thrusting during the Late Triassic and Early–Middle Jurassic (205–165 Ma) (Burchfiel et al., 1995; Huang et al., 2003; Wilson et al., 2006).

Magmatic rocks in the HSGB include Late Permian basaltic rocks (e.g., Song et al., 2004; Xiao and Xu, 2005), Late Triassic granitoids in the eastern HSGB (Fig. 1a) (Reid et al., 2007; Roger et al., 2003; Weislogel, 2008; Xiao et al., 2007; Yuan et al., 2010; Zhang et al., 2006a), and Jurassic granites and Miocene–Pleistocene volcanic rocks in the central-western HSGB (e.g., Hohxil area; Fig. 1b).

The newly discovered volcanic rocks are located in the northern Malan Mountains (Malanshan in Fig. 1b), northern Hohxil area (Fig. 1b). They occur as minor interbeds within the Norian (Late

Triassic) flysch that contains fossils of *Myophori (Castatoria) mansuyi Reed, Placunopsis remuensis Zhang, Cassianella cf. gryphaeala Munster* and *Plaeophyculastrigilata Goldfuss* (Zhu et al., 2003). The volcanic rocks are mainly massive andesites but minor interbeds of dacite (Appendix-1a) also occur in the flysch. In some outcrops, the volcanic rocks are distinctly more fragmented than the flysch (Appendix-1b).

3. Petrography

Both andesite and dacite samples exhibit porphyritic texture and signs of alteration. The andesites are bottle-green, and consist of augite (2–15 vol.%), plagioclase (15–25 vol.%), glassy cryptocrystal-line materials (40–60 vol.%), opaque minerals (Fe–Ti oxides) (5–10 vol.%), minor hornblende (1–5 vol.%) and secondary carbonate (2–8 vol.%). Except for minor phenocrysts, most mineral grains have diameters of 0.2–0.01 mm. The augite is mainly columnar (Appendix 1c and d), and can be divided into two groups based on size: relatively large grains (>15 μm) with core-rim structures and smaller (<15 μm) euhedral grains without obvious cores (Appendix 1e and f). Plagioclase is lath-shaped, and some grains (or parts of grains) were altered to fine sericite, chlorite or albite. The dacites are sage-green, and comprise 7 vol.% phenocrysts (1.2–0.20 mm; 6 vol.% plagioclase and 1 vol.% quartz), >90 vol.% matrices (<0.06 mm; 60–70 vol.% plagioclase, 10–15 vol.% cryptocrystalline-glassy materials, and 5–10 vol.% opaque minerals and minor zircon) and secondary carbonate (2–5 vol.%).

4. Analytical methods

Zircons were separated using conventional heavy liquid and magnetic separation techniques. Zircon grains were handpicked and mounted in an epoxy resin disk, and then polished. Their internal morphology was examined using cathodoluminescence prior to U-Pb isotopic analysis. The U-Pb isotopic analyses were performed using the LA-ICP-MS at the National Key Laboratory of Geological Processes and Mineral Resources, Faculty of Earth Sciences, China University of Geosciences (Wuhan). Detailed descriptions of the instrumentation and analytical accuracy for the LA-ICP-MS zircon U-Pb technique were given by Liu et al. (2010). The time-resolved spectra were processed off-line using ICPMSDATA software (Liu et al., 2010) to calculate the isotopic ratios using zircon 91500 as external standard. NIST SRM 610 was used as the reference material and ^{29}Si was used as internal calibrant. Common Pb was corrected by ComPbCorr#3 151 (Andersen, 2002) for those with common ^{206}Pb >1%. Uncertainties in the ages listed in Appendix 2 are cited as 1σ, and the weighted mean ages are quoted at the 95% confidence level.

Relatively fresh rock chips were selected for ^{40}Ar–^{39}Ar age analyses. They were ultrasonically cleaned successively in distilled water with <5% HNO$_3$ and then in distilled water, dried, and handpicked to remove visible contamination. Argon isotope analyses for four samples (2406a and 2121-6) were conducted on a MM-1200 mass spectrometer at the Laboratory of Analytical Center, Guilin Resource and Geological Institute following procedures similar to those described in Wang et al. (2007). The rock chips were wrapped in Sn foil and sealed in 6-mm-ID evacuated quartz–glass vials together with ZBH-25 (biotite) flux monitors, and irradiated for 37 h at the Beijing Nuclear Research Center. The monitor samples were individually fused and analyzed for argon-isotope compositions. All samples were step-heated using a radio-frequency furnace. Argon isotope analyses were conducted on a MM-1200 mass spectrometer at the Laboratory of Analytical Center, Guilin Resource and Geological Institute. The monitor standard was the ZBH-25 (biotite, 132.5 Ma). All errors are quoted at the 1σ level and do not include the uncertainly of the monitor age. The data are listed in Appendix 3.

Argon isotope analysis of sample (2406b and 2114-1) was conducted on a GV-5400 mass spectrometer at the State Key Laboratory of Isotope Geochemistry (SKLIG), Guangzhou Institute of Geochemistry, Chinese Academy of Sciences (GIG CAS). Rock chips of 30–60 meshes in size were ultrasonically cleaned first in distilled water with <5% HNO$_3$ and then in deionized water, and dried and handpicked to remove visible contamination. The sample and a monitor standard (ZBH-2506 with an age of 132.500 ± 0.663 Ma) were irradiated in the 49-2 reactor in Beijing for 54 h. Details of the analytical procedure used are given in Qiu and Jiang (2007). The ^{40}Ar–^{39}Ar dating results are calculated and plotted using the ArArCALC software of Koppers (2002). The ^{40}Ar–^{39}Ar age data are listed in Appendix 4.

Augite analyses and back-scattered-electron (BSE) imaging were carried out at the SKLIG GIG CAS with a JEOL JXA-8100 Superprobe. The operating conditions were as follows: 15 kV accelerating voltage, 20 nA beam current, 1–2 lm beam diameter, 10 s counting time and ZAF correction procedure for data reduction. The analytical procedures were described in detail by Huang et al. (2007). The augite composition data are listed in Appendix 5.

The samples chosen for elemental and isotopic analyses were first split into small chips and soaked in 4N hydrochloric acid for 1 h to remove secondary carbonate minerals, then powdered after rinsing with distilled water. Major element oxides (wt.%) were determined using a Varian Vista PRO ICP-AES at the SKLIG GIG CAS. Details of the analytical procedures were described by Li et al. (2002). Trace elements, including the rare earth element (REE), were analyzed using a Perkin-Elmer ELAN 6000 inductively-coupled plasma source mass spectrometer (ICP-MS) at the Key Laboratory of Isotope Geochronology and Geochemistry, Guangzhou Institute of Geochemistry, Chinese Academy of Sciences, following procedures described by Li et al. (2002). Analytical precision for most elements is better than 3%. The results are given in Appendix 6.

The Sr and Nd isotopic compositions were determined using a Finnigan MAT-262 Mass Spectrometer at the Institute of the Geology and Geophysics, Chinese Academy of Sciences, using essentially the same procedures as those of Zhang et al. (2002). The ^{87}Sr/^{86}Sr ratio of the NBS987 standard and ^{143}Nd/^{144}Nd ratio of the La Jolla standard measured during this study are 0.710246 ± 9 (2σm) and 0.511854 ± 8 (2σm), respectively. Overall blank contributions are about 0.2–0.5 ng for Rb and Sr, and about 50 pg for Nd and Sm. The Rb, Sr, Sm, and Nd concentrations exhibit good agreement with those analyzed using ICP-MS. The measured ^{143}Nd/^{144}Nd and ^{86}Sr/^{88}Sr ratios are normalized to ^{146}Nd/^{144}Nd = 0.7219 and ^{86}Sr/^{88}Sr = 0.1194, respectively. The results are given in Appendix 6.

Platinum group elements (PGE) were analyzed by inductively coupled plasma mass spectrometry (ICP-MS) following the nickel sulfide fire assay method of Sun and Sun (2005) at the SKLIG GIG CAS. Briefly, a sample of 15 g was spiked with a solution isotopically enriched in ^{190}Os and ^{185}Re, and fused with Na$_2$B$_4$O$_7$ flux in a muffle furnace for preconcentration of PGE into a sulfide button. The button was dissolved by HCl for collecting PGE residue. Os was separated from the PGE residue using distillation and absorbed by pure water. The remainder was prepared for determination of Ru, Rh, Pd, Ir, Pt and Re contents. The procedural blank is 2 ppt for Os, 6 ppt for Ru, 1 ppt for Rh, 28 ppt for Pd, 1.5 ppt for Ir, 18 ppt for Pt and 20 ppt for Re. The results are given in Appendix 6.

5. Results

5.1. Geochronology

Backscattered Electron Imaging (BSE) images of analyzed zircons (dacite sample 2406a) show that most are elongated crystals with some cracks, but a few grains display clear magmatic oscillatory zonings (Fig. 2a). Except for one analyzed spot with low Th/U ratios (0.02), the other 29 LA-ICPMS analyzed spots have U contents between 191 and 5288 ppm and Th contents between 73 and 6608 ppm,
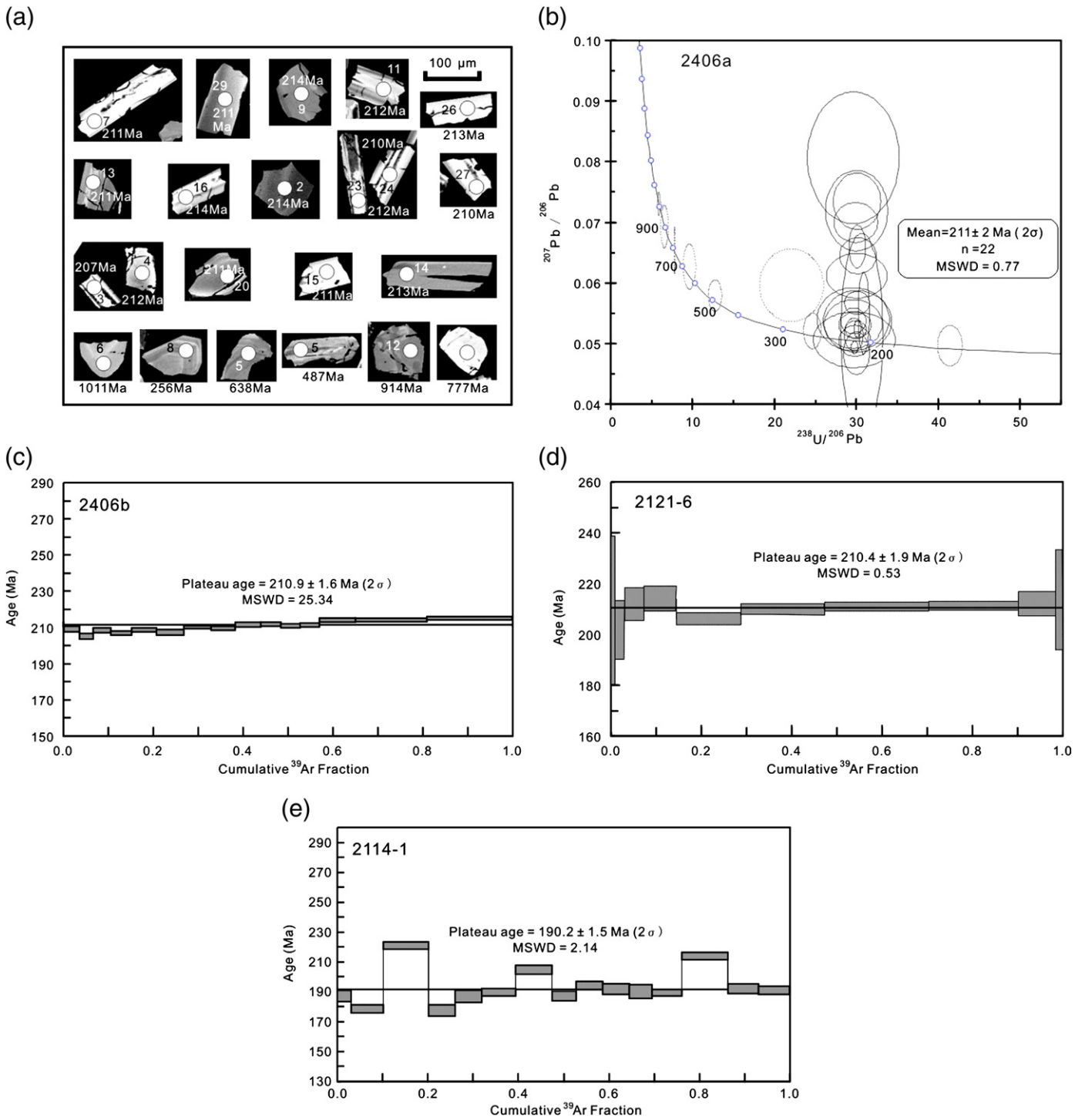
(a)

(b)

(c)

(d)

(e)

Fig. 2. LA-ICP-MS zircon U-Pb Tera–Wasserburg diagram with BSE images for sample 2406a (a and b), and the $^{40}Ar/^{39}Ar$ age spectra diagrams for the Hohxil dacite sample (c) and high-Mg andesite sample 2121-6 (d) and 2114-1(e).

resulting in variable but higher Th/U ratios (0.19–1.46). Twenty-two spot results have a weighted mean $^{206}Pb/^{238}U$ age of 211 ± 2 Ma (2σ) (MSWD = 0.77), interpreted as the dacite formation age. Although one spot has a $^{206}Pb/^{238}U$ age younger than 211 Ma (154 ± 2 Ma), possibly due to contamination, the remaining 7 spots have greater, and largely concordant, ages (250–1010 Ma) (Fig. 2b). We interpret these older zircons to be inherited zircons.

Andesite and dacite ages were also determined using argon isotope analyses in two different argon geochronological laboratories,

using the step-heating method. Dacite sample 2406b yielded a whole-rock $^{40}Ar/^{39}Ar$ weighted mean plateau age of 210.9 ± 1.6 Ma (Fig. 2c), which is consistent with the zircon U-Pb age (211 ± 2 Ma) of sample 2406a (Fig. 2b). Andesite sample 2121-6 yielded a whole-rock $^{40}Ar/^{39}Ar$ weighted mean plateau age of 210.4 ± 1.9 Ma (Fig. 2d). Another andesite sample (2114-1) failed to yield an acceptable $^{40}Ar/^{39}Ar$ plateau (Fig. 2e). The $^{40}Ar/^{39}Ar$ weighted mean plateau ages of 210.4 ± 1.9 Ma is interpreted as the eruption age of the andesites, which is almost identical to the age of the dacite.
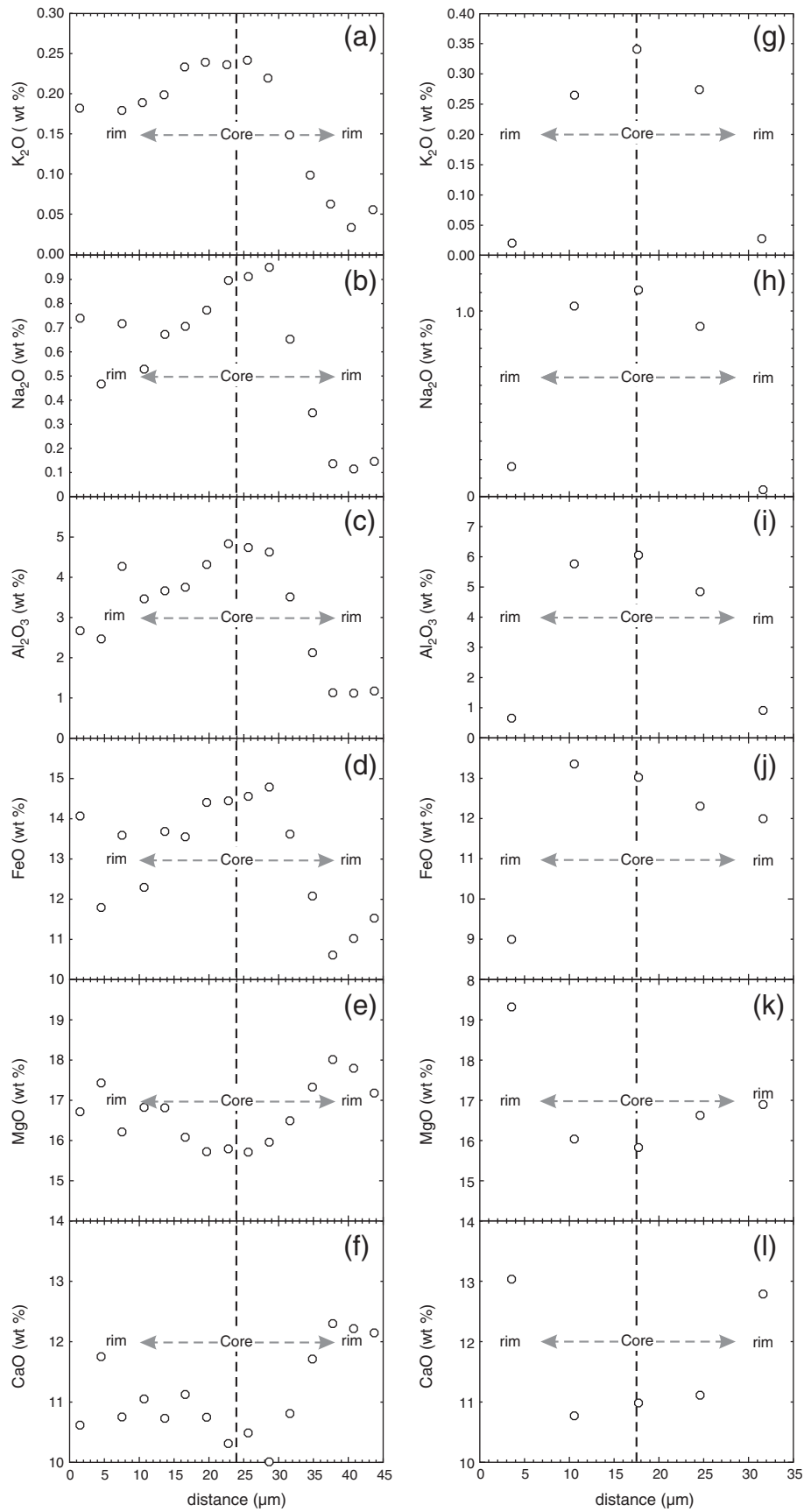
Fig. 3. Augite composition section diagrams for two typical grains with core-rim structure (Appendix 1e and f).

5.2. Pyroxene compositions

Compositional data for augites are shown in Appendix 1g. Some large augite crystals (>15 μm) with core-rim structures (Appendix 1e and f) exhibit regular composition changes from cores to rims (Fig. 3): FeO, Na_2O and Al_2O_3 decrease, and MgO and CaO increase. In addition, the cores of such crystals have higher FeO, Na_2O and Al_2O_3 but low $Mg^\#$ ($100 \times Mg^{2+}/(Mg^{2+} + Fe^{2+})$) and CaO values than their rims (Fig. 4). Moreover, data from all augites, including the relatively small grains (<15 μm) that show no clear core-rim structures, define linear compositional trends where FeO, Na_2O and Al_2O_3 decrease and CaO increases with increasing $Mg^\#$ (Fig. 4).

5.3. Alteration effects

The andesite and dacite samples have variable LOI (loss on ignition) reflecting variable $H_2O + CO_2$ contents (1.70–7.34 wt.%) (Appendix 6), probably due to differing degrees of alteration (Wang et al., 2006b). Their K_2O, Na_2O, CaO (Appendix 7a–c) and large ion lithophile element (e.g., Rb, and Ba) contents increase with increasing LOI ($H_2O + CO_2$ contents) (Appendix 8a–b), indicating that their abundances have been changed by alteration (e.g., Wang et al., 2006b). Their Sr contents exhibit no obvious trend with increasing LOI (Appendix 8c). The ($^{87}Sr/^{86}Sr$)$_i$ ratio of the dacite sample with the highest LOI is greater than that of the relatively low-LOI sample (Appendix 8l) but andesite samples do not show a similar relationship. MgO, FeO^T ($= Fe_2O_3 \times 0.9 + FeO$), Al_2O_3, TiO_2, P_2O_5 (Appendix 7d–h) and transition (e.g., Cr), rare earth (e.g., La and Yb), and high field-strength (e.g., Th and Ta) element contents, related element–element ratios (e.g., Nb/La and Nb/Ta) (Appendix 8d–j) and εNd(t) values (Appendix 8k) for all andesite and dacite samples show no obvious variation with increasing LOI ($H_2O + CO_2$ contents), indicating that their contents probably have not been modified by alteration (Wang et al., 2006b; Zhou, 1999). Thus, immobile elements such as MgO, FeO^T, Al_2O_3, TiO_2, P_2O_5, transition elements (e.g., Cr, Ni), high-field-strength elements (HFSE) (Ti, Zr, Y, Nb, Ta, Hf, Th), rare earth elements (REE), and Nd isotope compositions are mainly used in the following discussion. Andesite Sr contents and Sr isotope compositions are also considered.

5.4. Major and trace element compositions

The northern Hohxil Triassic volcanic samples plot in the field of andesites and dacites on a plot of SiO_2 (wt.%) vs. Zr/TiO_2 (Fig. 5a). Although their K_2O contents may have been increased by late-stage alteration (Appendix 7a), the samples still plot in the field of low- and medium-K calc-alkaline series magmatic rocks (Fig. 5b). They also plot in the field of Low-Fe magmatic rocks (Fig. 5c). The andesite samples exhibit high MgO (5.83–8.88 wt.%), $Mg^\#$ (64–72), and Cr (272–531 ppm) and Ni (66.7–636 ppm) contents, which are similar to typical Cenozoic high-Mg andesites in arc settings, e.g., "adakitic" and "Piip" high-Mg andesites in the Aleutian islands (Alaska) and the Kamchatka Strait to the west of the Aleutian islands (e.g., Yogodzinski et al., 1994, 1995, 2001; Yogodzinski and Kelemen, 1998), bajaites in Baja California (Mexico) (Calmus et al., 2003; Saunders et al., 1987), sanukitoids in the Setouchi Volcanic Belt (SW Japan) (Shimoda et al., 1998; Tatsumi, 2001; Tatsumi and Ishizaka, 1981) and boninites of the Bonin Islands (Japan) (e.g., Taylor et al., 1994; Umino, 1986) (Fig. 6a–e). However, they are different from boninites in that they exhibit higher TiO_2 (0.48–0.57) and Al_2O_3 (13.95–15.80 wt.%) contents (Fig. 6f). The dacite samples have distinctly lower MgO (0.87–1.14 wt.%) and TiO_2 (0.20–0.25 wt.%) contents, $Mg^\#$ (50–54), and compatible element Cr (24.7–46.8 ppm) and Ni (2.28–61.9 ppm) contents, but slightly higher Al_2O_3 (15.54–16.36 wt.%) contents (Fig. 6; Appendix 6).

Both the Hohxil andesites and dacites are enriched in light rare earth elements (LREE), but depleted in heavy REE (HREE) and Nb and Ti (Fig. 7a and b). However, the dacites exhibit more pronounced HREE depletions than the andesites (Fig. 7a and b). Moreover, the dacites have negligible to positive Eu anomalies, but the andesites have slightly negative Eu anomalies (Fig. 7a). Compared with Cenozoic high-Mg arc andesites, the Hohxil andesites have REE and trace element patterns similar only to the Setouchi sanukitoids (Fig. 7a and b). They also have La/Yb (6.1–11.9), Th/La (0.36–0.59) and Nb/Ta (11–13) ratios similar to the Setouchi sanukitoids (Fig. 5d–f). Both the Hohxil andesite and the
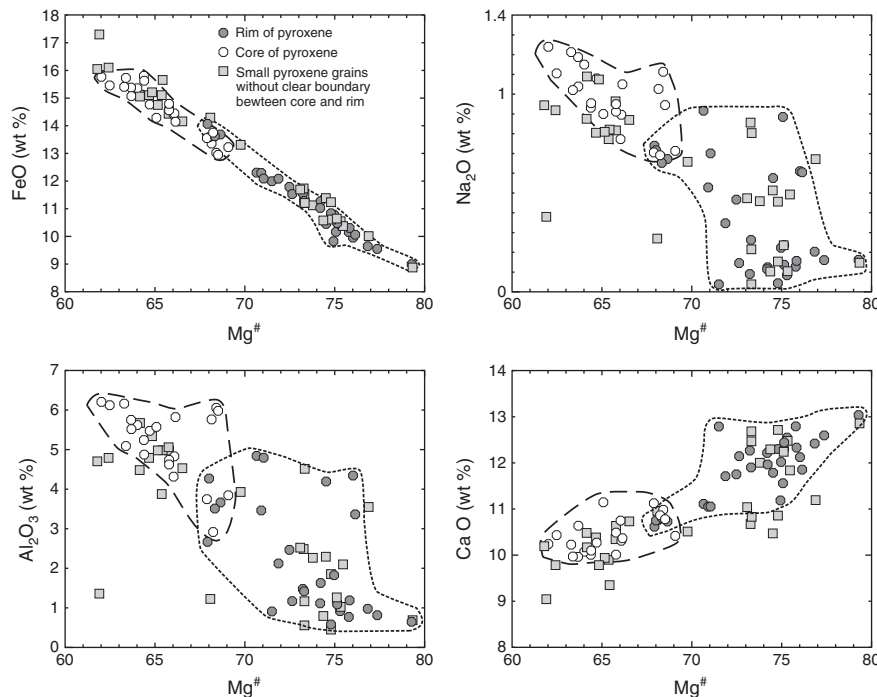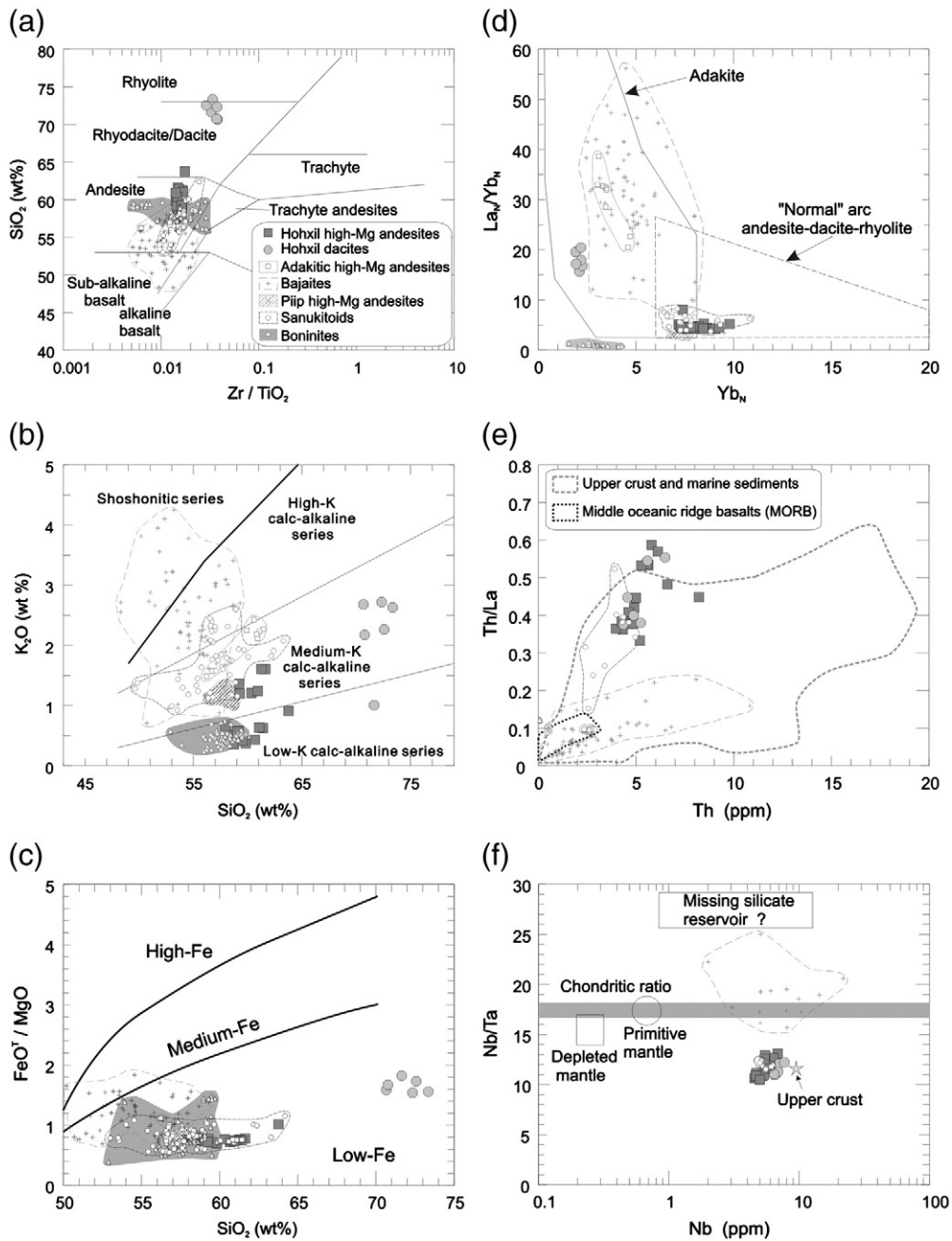

Fig. 4. Augite composition diagrams.

Fig. 5. (a) SiO_2 vs. Zr/TiO_2 (Winchester and Floyd, 1977); (b) K_2O vs. SiO_2 (Peccerillo and Taylor, 1976); (c) FeO^T ($FeO + 0.9 \times Fe_2O_3$)/MgO vs. SiO_2 (Arculus, 2003); (d) La_N/Yb_N vs. Yb_N (Drummond and Defant, 1990); (e) Th/La vs. Th (Plank, 2005); (f) Nb/Ta vs. Nb (Rudnick et al., 2000). Upper crust and marine sediments are from Plank (2005), Plank and Langmuir (1998), and references therein. MORB data are from Niu and Batiza (1997). The data for sanukitoids in SW Japan are from Shimoda et al. (1998), Tatsumi (2001), Tatsumi and Ishizaka (1981), and references therein. The data for Bonin Island boninites are from Taylor et al. (1994) Umino (1986), and references therein. The data for bajaites in the Baja area, California, Mexico are from Calmus et al. (2003) and Saunders et al. (1987). The data for Adakitic high-Mg andesites of Adak Island (Aleutian islands) and the Kamchatka Strait to the west of Aleutian islands are from Yogodzinski et al. (1995, 1998, 2001), and references therein; the data for Piip-type high-Mg andesites of the Piip volcano (Aleutian islands) are from Yogodzinski et al. (1994). HMA-high Mg andesites.

Setouchi sanukitoid samples plot in the transition field between adakites and "normal" arc andesite–dacite–rhyolite suites (Fig. 5d), and exhibit high Th/La ratios and low Na/Ta ratios that approximate those of marine sediments and upper continental crust (Fig. 5e and f). All the Hohxil dacite samples plot in the field of typical slab-derived adakites (Defant and Drummond, 1990) (Fig. 5d).

5.5. Platinum group elements (PGE) and Re and Au

The Hohxil andesites have total PGE abundance ranging from 0.382 ppb in sample 2114-1 to 3.16 ppb in sample 2121-2. They have strongly fractionated PGE patterns (Fig. 8a) with a clear increase in primitive mantle-normalized concentrations from the Ir group (Os, Ir, and Ru) PGEs to Pd group (Rh, Pt and Pd) PGEs, Au and Re. They also have negligible or slightly negative Ir, slightly positive Pt, and variable Au anomalies. However, except for Au, their PGE patterns are approximately subparallel (Fig. 8a). The Hohxil dacites have distinctly lower PGE abundance (0.093–0.095 ppb), but also exhibit strongly fractionated PGE patterns with significant fractionation between both Ir- and Pd-group PGEs (Fig. 8a). They also have slightly negative Ir and slightly positive Pt and Au anomalies (Fig. 8a). Both andesites and dacites exhibit high Pt/Pt* (Pt anomaly), $(Pt/Ir)_N$ and Re/Os ratios higher than those of chondrites and primitive mantle (Barnes et al., 1988; McDonough and Sun, 1995), but similar to those of the
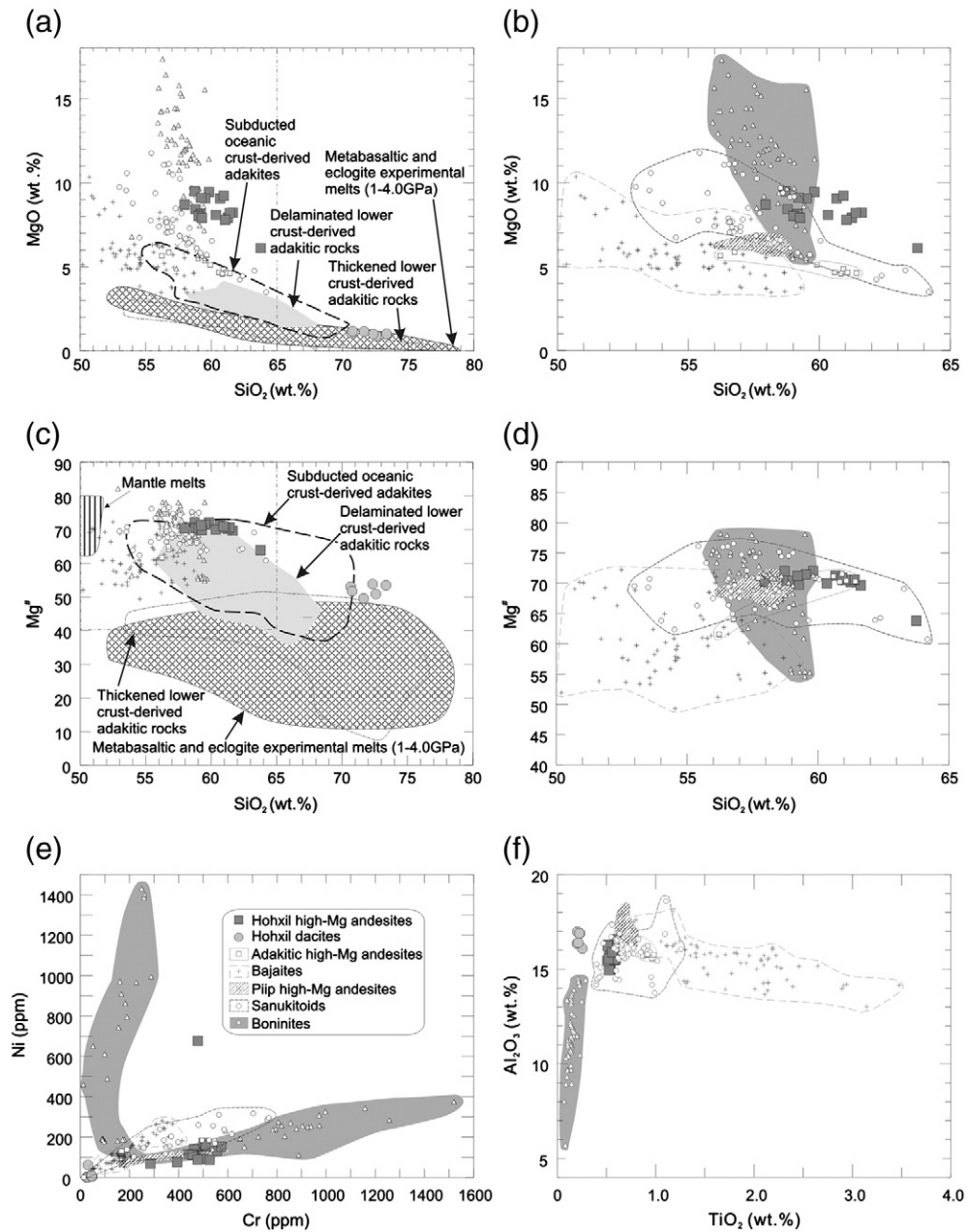
Fig. 6. (a and b) SiO$_2$ vs. MgO; (c and d) SiO$_2$ vs. Mg$^{\#}$; (e) Ni vs. Cr; (f) Al$_2$O$_3$ vs. TiO$_2$. The field of metabasaltic and eclogite experimental melts (1.0–4.0 GPa) is from the following references (Rapp et al., 1999, 2003, and references therein). The fields for delaminated lower crust, subducted oceanic crust, and thickened lower crust-derived adakitic rocks are after Wang et al. (2006a, b). See Fig. 5 for other data sources.

pyroxenite veins in the Kamchatka arc mantle peridotites and close to those of the Kamchatka arc adakites (Kepezhinskas et al., 2002) (Fig. 8b and c).

5.6. Nd–Sr isotope compositions

The Hohxil andesites and dacites have high initial ^{87}Sr/^{86}Sr isotopic ratios (0.7086 to 0.7107) and low εNd(t) values (−7.57–−9.59), which are different from those of Late-Permian mafic rocks and Neoproterozoic igneous and metamorphic rocks in the eastern Songpan–Ganzi and western Yangtze Blocks, and Triassic granitoids in the eastern HSGB (Fig. 9a, b). However, their Nd–Sr isotope compositions are similar to those of modern marine sediments and Proterozoic–Triassic sediments in the HSGB (Fig. 9a, b). In addition, their isotopic compositions also partially overlap those of the Triassic

Kunlun intrusive rocks and magmatic rocks in the Qiangtang and Yidun area (Fig. 9a, b).

6. Discussion

6.1. Petrogenesis

Triassic andesites and dacites in the Hohxil area are geochemically similar to high-Mg andesites and adakitic rocks, respectively (Figs. 5–7). There are different models accounting for the petrogenesis of such high-Mg andesite–adakitic rock suites, including assimilation fractional crystallization (AFC) or fractional crystallization (FC) from parental basaltic magmas (Castillo et al., 1999; Macpherson et al., 2006), magma mixing between felsic and basaltic magmas (e.g., Streck et al., 2007), and interaction between melts and mantle (e.g., Gao et al., 2004; Kay et al., 1993; Shimoda et al., 1998; Tatsumi, 2001; Tatsumi and Hanyu, 2003;
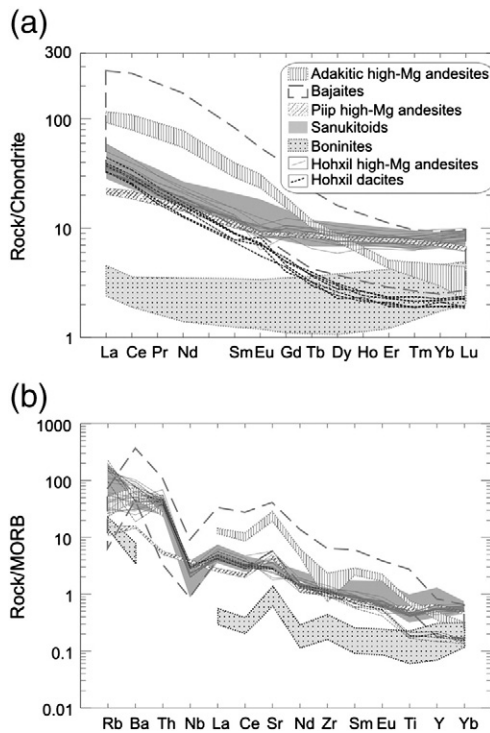
Fig. 7. (a) Chondrite-normalized rare earth element (REE) patterns for the Hohxil high-Mg andesites and dacites. Chondrite normalizing values are from Boynton (1984). (b) Middle oceanic ridge basalt (MORB)-normalized trace element patterns for the Hohxil high-Mg andesites and dacites. MORB normalizing values are from Sun and McDonough (1989). See Fig. 5 for other data sources.

Xu et al., 2008; Yogodzinski et al., 1994, 1995; Yogodzinski and Kelemen, 1998).

We argue that the first two models are not applicable to the Hohxil high-Mg andesite–adakitic rock suites based on the following observations. First, the Hohxil dacites, including a sample with the lowest LOI or $H_2O + CO_2$ content (indicating the least alteration), exhibits initial $^{87}Sr/^{86}Sr$ isotopic ratios slightly lower than those of the high-Mg andesites (Appendix 8l and Fig. 9), which is inconsistent with AFC or magma mixing models (Castillo et al., 1999; Streck et al., 2007). A positive correlation between Th/Nb and $\varepsilon Nd(t)$ values (Fig. 8d) and a negative correlation between Th/Nb and La/Sm ratios (Fig. 8e) for the Hohxil high-Mg andesite–adakitic rock suites are also inconsistent with extensive crustal contamination (Condie, 2003; Puchtel et al., 1997). Second, geochemical disequilibrium (e.g., low $Mg^{\#}$ core and high $Mg^{\#}$ rim) during the crystallization of augites in the Hohxil high-Mg andesites (Appendix 1e, f; Figs. 3–4), not only argues against low-$Mg^{\#}$ crustal material assimilation, but also is inconsistent with the compositions (e.g., low-$Mg^{\#}$ rim and high $Mg^{\#}$ interior) of zoned augites from magma mixing-derived high-Mg andesites (Streck et al., 2007). Third, PGE (e.g., Ir) contents do not decrease with increasing Th contents (an indicator of the degree of fractionation) (Fig. 8f), and the PGE patterns of the Hohxil high-Mg andesites are subparallel (Fig. 8a), indicating that variations in their PGE content are not related to sulfide fractional crystallization (Setiabudi et al., 2007). Fourth, the Hohxil high-Mg andesite–adakitic

rock suites are not associated with contemporary basaltic rocks that would correspond to the required mafic end member in AFC, FC and magma mixing models (e.g., Castillo et al., 1999; Macpherson et al., 2006; Streck et al., 2007). Finally, there is a clear compositional gap between high-Mg andesites ($SiO_2 = 54$–60 wt.%) and dacites ($SiO_2 = 67$–71 wt.%) (Figs. 5 and 6), which is inconsistent with the continuous compositional trend implied by AFC, FC or magma mixing processes (Castillo et al., 1999; Macpherson et al., 2006; Streck et al., 2007).

Zoned augite compositions in the Hohxil high-Mg andesites exhibit, from core to rim, a decrease in K_2O, Na_2O, Al_2O_3 and FeO and an increase in MgO and CaO (Figs. 3–4). The compositional disequilibrium characteristics of the augites suggest that the Hohxil high-Mg andesites were likely derived by interaction between melts and mantle (e.g., Rapp et al., 1999; Yogodzinski and Kelemen, 1998). However, the origin of the melts requires further clarification, given that similar melts have been attributed to partial melting of delaminated or subducted continental crust (e.g., Gao et al., 2004; Wang et al., 2006b, 2008c; Xu et al., 2008), subducted basaltic oceanic crust, or sediments (e.g., Kay et al., 1993; Kelemen et al., 2003; Shimoda et al., 1998; Tatsumi, 2001; Tatsumi and Hanyu, 2003; Yogodzinski and Kelemen, 1998; Yogodzinski et al., 1994, 1995).
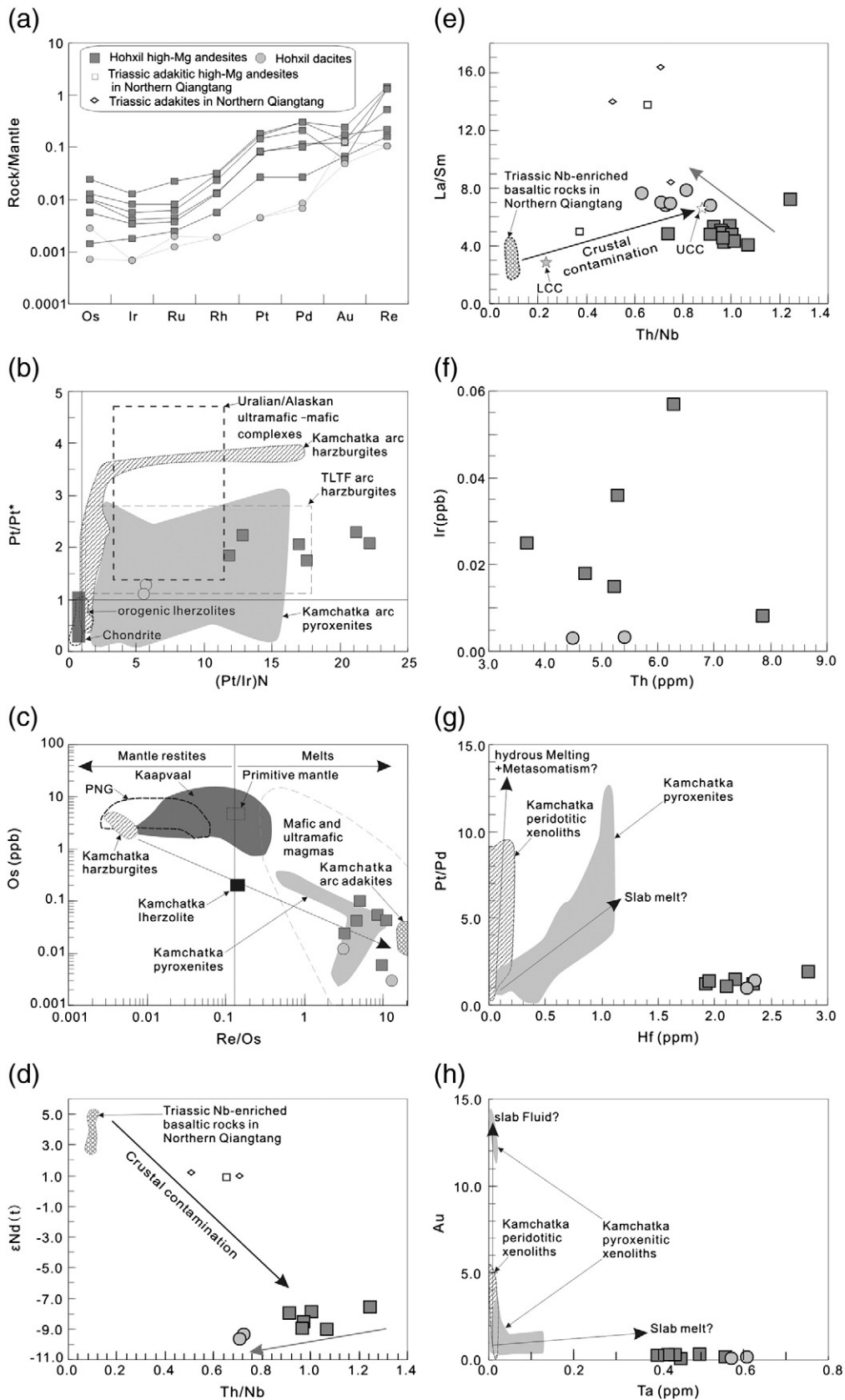
The Hohxil high-Mg andesite and dacite suites exhibit lower εNd (t) values and higher initial $^{87}Sr/^{86}Sr$ isotopic ratios than those of the Late-Permian mafic rocks and Neoproterozoic igneous and metamorphic rocks in the eastern HSGB and western Yangtze Blocks or Triassic granitoids in the eastern HSGB (Fig. 9), indicating that they were not generated by the interaction of melts derived from delaminated or subducted continental middle-lower crust with mantle peridotites. They also have significantly lower $\varepsilon Nd(t)$ values and higher initial $^{87}Sr/^{86}Sr$ isotopic ratios than Late Triassic northern Qiangtang high-Mg andesite–adakite suites that were generated by interactions between subducted basaltic oceanic crust-derived melts and mantle wedge peridotites (Fig. 8d–e) (Wang et al., 2008b), indicating that their formation was not related to partial melting of subducted basaltic oceanic crust.

We suggest that the Hohxil high-Mg andesite and dacite suites were probably generated by the interaction of subducted oceanic sediment-derived melts and mantle peridotites on the basis of the following evidence. First, they exhibit relatively low $\varepsilon Nd(t)$ values and high initial $^{87}Sr/^{86}Sr$ isotopic ratios (Fig. 9), high Th/La (Fig. 5e) and Th/Nb (Fig. 8d) ratios, and low Na/Ta (Fig. 5f) ratios, similar to those of Proterozoic–Triassic sediments in the HSGB, modern marine sediments or the upper continental crust. The Hohxil high-Mg andesites are geochemically similar to Cenozoic sanukitoids in the southwestern Japan arc (Figs. 5–7), which are considered to have been generated by the interaction of subducted oceanic sediment-derived melts and mantle peridotites (Shimoda et al., 1998; Tatsumi, 2001; Tatsumi and Hanyu, 2003). Second, the Hohxil high-Mg andesite and dacite suites have PGE compositions similar to those of slab melt-metasomatized pyroxenite veins in Kamchatka arc mantle peridotites, and comparable to those of Kamchatka arc adakites (Kepezhinskas et al., 2002) (Fig. 8b and c). Moreover, they also exhibit a PGE compositional trend consistent with the involvement of slab melt rather than slab fluid (Kepezhinskas et al., 2002) (Fig. 8g and h). As a result, we suggest that the slab melt was generated by the partial melting of subducted oceanic sediments.

Fig. 8. (a) Mantle-normalized PGE abundances for the Hohxil high-Mg andesites and dacites. Mantle values are from Barnes et al. (1988). (b) Pt/Pt* (Pt anomaly) vs. $(Pt/Ir)_N$ diagram for the Hohxil high-Mg andesites and dacites. The harzburgite and pyroxenite xenolith from the magmatic rocks of the Kamchatka arc (Russia) and the Tabar–Lihir–Tanga–Feni (TLTF) arc (Papua New Guinea), orogenic lherzolite, and Uralian/Alaskan zoned ultramafic — mafic complexe fields are after Kepezhinskas et al. (2002), and references therein. The Pt anomaly $(Pt/Pt^* = Pt_N/Rh_N \times Pd_N)$ provides a measure of the deviation of Pt concentration from the general trend of the primitive mantle-normalized pattern of a sample. C1 chondrite normalizing values for Pt and Ir (Pt/Ir ratio) are from McDonough and Sun (1995). (c) Re/Os vs. Os concentrations for the Hohxil high-Mg andesites and dacites. The fields for ultramafic xenoliths from the Kamchatka arc and the Papua New Guinea (PNG) arc system, Kaapvaal craton peridotites, mantle-derived mafic and ultramafic magmas, and primitive mantle values are after Kepezhinskas et al. (2002). (d) ε_{ND} (t) vs. Th/Nb diagram. (e) La/Sm vs. Th/Nb diagram. Data for LCC (lower continental crust) and UCC (upper continental crust) are from Rudnick and Gao (2003). (f) Ir vs. Th; (g) Pt/Pd vs. Hf. (h) Au vs. Ta. The fields for ultramafic xenoliths from the Kamchatka arc are after Kepezhinskas et al. (2002).

The composition of a sediment-derived melt can change from rhyolitic to andesitic as it dissolves olivine and clinopyroxene in mantle peridotites (Tatsumi, 2001). The Hohxil dacites exhibit slightly higher Mg# (50–54) than those (<0.47) of metabasaltic and eclogite or metasedimentary rock experimental melts (1–4.0 GPa) (Fig. 6a–d) (e.g., Rapp et al., 1999; Schmidt et al., 2004), indicating that the dacite magmas were slightly hybridized by mantle peridotite during ascent. However, the Hohxil high-Mg andesites have distinctly higher Mg#
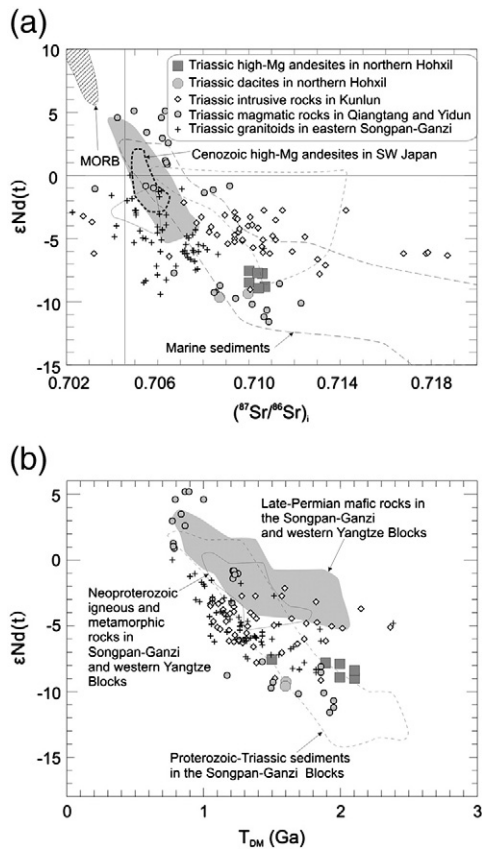
Fig. 9. (a) Nd–Sr and (b) Nd isotope diagrams for the Hohxil high-Mg andesites and dacites. The fields for the Neoproterozoic igneous and metamorphic rocks in the Songpan–Ganzi and west Yangtze Blocks, Proterozoic–Triassic sediments in the Songpan–Ganzi Block, Late-Permian mafic rocks in the Songpan–Ganzi and west Yangtze Blocks are after Wang et al. (2008c). The data for marine sediments are from Plank and Langmuir (1998). The Nd–Sr isotope data for Triassic magmatic rock in the central-northern Tibetan Plateau are from these references (Fu et al., 2010; Harris et al., 1988; Roger et al., 2003, 2004; Wang et al., 2008b; Xiao et al., 2007; Yuan et al., 2009, 2010; Zhang et al., 2006a, 2007a,b, and references therein).

(64–72) and compatible element (e.g., Ni) contents (Fig. 6a–e), suggesting that their magmas were strongly hybridized.

Sediment melting models have primarily been applied to arc settings involving subduction of oceanic crust containing sediments (Johnson and Plank, 1999; Plank, 2005). The HSGB is a triangular tectonic unit, which is broad in the east and narrow in the west. The basement in the eastern end of the HSGB may be of continental, South China, affinity (Burchfiel et al., 1995; Li et al., 2003; Roger and Calassou, 1997; Yin and Harrison, 2000). In addition, some studies also suggest that middle–late Permian pillow basalts immediately overlie Early Permian platform carbonates and clastics, and are in turn overlain by Triassic flysch in the eastern HSGB (Song et al., 2004; Xiao and Xu, 2005). Therefore, as suggested by Zhang et al. (2006a), the eastern HSGB may be a continental peninsula extending into the Paleo-Tethys Ocean from the South China margin. However, for the central-western HSGB, geophysical (Wittlinger et al., 1996) and geological (e.g., Roger et al., 2003) data suggest that oceanic crust may underlie the thick Triassic flysch sequence. It is possible that during the Triassic subduction of the central-western Songpan–Ganzi oceanic basin, the ocean floor basalts began to dehydrate under eclogite facies conditions. As sediments on top of the subducting oceanic crust have a relatively low solidus (H_2O+Cl fluid-saturated) at high-pressure ($775\pm25\ ^\circ C$ at 2 GPa; Johnson and Plank, 1999), the ascending fluids from the dehydrated basaltic oceanic crust triggered sediment melting and the generation of adakitic magmas (i.e., the Hohxil

dacites). Adakitic magmas can generally be produced by melting of mafic materials, leaving residual phases that include garnet ± rutile but little or no plagioclase (Rapp et al., 1999, 2003; Xiong et al., 2005). Pelitic sediments and greywackes have the same eclogitic mineralogy (but different mineral proportions) as basaltic rocks at depths >70–100 km (i.e., 2.0~3.5 GPa; Schmidt et al., 2004). Experimental data suggest that sediment-derived melts in equilibrium with garnet are markedly depleted in HREE and enriched in LREE (Johnson and Plank, 1999). When such melts interact with mantle peridotites during ascent, the result is likely to be magmas comparable to the Triassic Hohxil high-Mg andesite–dacite suites.

6.2. Tectonic implications

Four main basin models have been proposed for the Songpan–Ganzi Triassic strata: (1) intercontinental rift basin; (2) back-arc basin, (3) foreland basin and (4) remnant oceanic basin. In this first model, the Songpan–Ganzi basin originated from the Late Paleozoic–Triassic rifting of the South China Block from the South Qinling or the western margin of the South China Block (e.g.,Song et al., 2004). The Late Permian Emeishan mantle plume on the western margin of the South China Block is considered to have caused the inferred rifting (e.g., Chung and Jahn, 1995; Song et al., 2004). In the second model, the Songpan–Ganzi basin is interpreted as a back-arc basin between the Kunlun arc to the north and the outboard Yidun arc to the south (e.g., Burchfiel et al., 1995; Pullen et al., 2008; Şengör et al., 1988; Watson et al., 1987) (Fig. 1). The Kunlun and Yidun arcs are generally considered to result from the northward subduction of the Paleo-Tethyan oceanic basin along the Anyimaqen–Kunlun–Muztagh suture and the northeastward or northward subduction of the Jinshajiang oceanic basin along the Jinshajiang suture, respectively (Fig. 1). Pullen et al. (2008) proposed an alternative back-arc basin model where, after middle Triassic collisions between the North China and South China Blocks and between the Qiangtang and Paleo-Tethys arc terranes, collision-induced oceanic slab rollback led to rifting of the eastern Kunlun terrane (Yidun arc) from Eurasia and opening of a back-arc basin in which Songpan–Ganzi flysch was deposited. Late Triassic arc fragments (e.g., Yidun) and the Songpan–Ganzi flysch were then accreted to the Qiangtang terrane and South China Block. Recently, based on Triassic (224–205 Ma) intrusive rocks in the eastern HSGB, Yuan et al. (2010) proposed that the Songpan–Ganzi basin was similar to a foreland basin formed in response to an arc-continental collision and the resultant flexure and fracturing of western South China Block lithosphere. A remnant-ocean basin model has also been commonly invoked for the evolution of whole Songpan–Ganzi basin (Nie et al., 1994; Weislogel, 2008; Weislogel et al., 2006; Yin and Harrison, 2000; Zhou and Graham, 1996). In this model, (1) crustal shortening and thrust-sheet development associated with North China–South China collision caused loading and flexural subsidence of the subducting lower plate (oceanic crust?) where Triassic sediment accumulation took place (Fig. 3b of Weislogel, 2008); or (2) the double-sided subduction of the Songpan–Ganzi oceanic basin under the Kunlun–Qaidam Block in the north and the Qiangtang Block in the south or west took place during the Triassic (Nie et al., 1994; Roger et al., 2003; Yin and Harrison, 2000).

However, as most previous studies concerning the Triassic evolution of the HSGB have concentrated on the tectonically complex eastern part of the block (Fig. 1a), there are important issues that remain to be resolved, including (1) the relationship between late Permian basaltic magmatism and the mantle plume activity in western South China (Chung and Jahn, 1995; Song et al., 2004; Xiao and Xu, 2005), and (2) the polarity or direction and timing of the different subduction systems (Burchfiel et al., 1995; Nie et al., 1994; Pullen et al., 2008; Reid et al., 2007; Roger et al., 2004; Şengör et al., 1988).

The Songpan–Ganzi basin extends more than 2500 km along an east–west trend (according to Fig. 2 of Yin and Harrison (2000)) and

displays considerable geological variation along its length. In contrast to the eastern part of the basin, the central-western part contains no old (e.g., Neoproterozoic) metamorphic basement rocks with South China affinity or arc fragments (similar to the Yidun arc) and few Triassic intrusive rocks. It is also situated in a comparatively simple tectonic setting, i.e., between the Kunlun–Qaidam and Qiangtang Blocks (Fig. 1a). Therefore, models developed based on eastern HSGB studies may not fully characterize the coeval evolution of the central-western HSGB.

The volcanic rocks of this study are located in the central-western HSGB between the Kunlun–Qaidam and the Qiangtang Blocks (Fig. 1). As mentioned above, the northern Hohxil high-Mg andesites are very similar to sanukitoids in the Cenozoic arc of southeastern Japan, and the high-Mg andesite and dacite suites also originated from subducted oceanic sediments and subsequent interaction between melts and mantle peridotite. Therefore, we suggest that they were most probably generated in a Triassic arc setting. The fact that these rocks occur close to the Late Permian–Triassic or Early Jurassic Anyimaqen–Kunlun–Muztagh suture (e.g., Roger et al., 2003; Yin and Harrison, 2000) (Fig. 1) suggests that they were related to the northward subduction of Songpan–Gangzi oceanic crust. Moreover, there is an east–west-trending belt of Triassic (250–207 Ma) arc magmatic rocks in the southern Kunlun Block (Fig. 1a), indicating that the Songpan–Gangzi oceanic basin subducted beneath the southern Kunlun Block at that time (Fig. 10) (Harris et al., 1988; Xiao et al., 2002a,b; Yin and Harrison, 2000; Yuan et al., 2009).

In addition, an east–west belt of Triassic (250–207 Ma) magmatic rocks have recently been reported in central and northern Qiangtang Block (e.g., Fu et al., 2010; Wang et al., 2008a,b), including the Yidun arc (Reid et al., 2007; Roger et al., 2003; Weislogel, 2008) (Fig. 1a). This Triassic belt can best be interpreted as a magmatic arc. As these magmatic rocks commonly occur to the south of the Jinshajiang suture in the central-western Qiangtang Block and west of the Ganzi–Litang suture in the eastern region (Fig. 1a), the Songpan–Ganzi oceanic basin must also have subducted southward or westward beneath the northern Qiangtang Block (Fig. 10). Triassic (219–236 Ma) adakite–magnesian andesite–Nb-enriched basaltic rock associations in the Tuotuohe area, central Qiangtang terrane further confirms the occurrence for partial melting of the Songpan–Ganzi oceanic slab and subsequent interaction between slab melts and mantle peridotites (Wang et al., 2008b).

In summary, we suggest that, during the Triassic, the Songpan–Ganzi oceanic basin subducted both northward under the Kunlun–Qaidam Block and southward or westward under the Qiangtang Block, respectively (Fig. 10), as suggested by some previous workers based on tectonic, sedimentary, metamorphic and paleomagnetic analyses (e.g., Kapp et al., 2003; Nie et al., 1994; Reid et al., 2007; Roger et al., 2003; Yin and Harrison, 2000). With the ongoing double-sided subduction, the eastern Songpan–Ganzi oceanic basin diminished in size or even disappeared, and collisions between different blocks or arc

fragments (e.g., the South China, Kunlun–Qaidam, North China, South Qinling, Qilian, Yidun, and Qiangtang Blocks; Fig. 1a) occurred. A new basin began to develop in response to an arc-continent collision that was accompanied by the flexure and fracturing of the western South China Block lithosphere (Yuan et al., 2010). Although the central-western Songpan–Ganzi oceanic basin became smaller during this period, it did not disappear entirely and may have undergone flexure due to compression (Fig. 10) (Weislogel, 2008; Zhou and Graham, 1996).

Thus, the Triassic flysch deposits in the Songpan–Ganzi basin underwent tectonic thickening, and rapid erosion of the Qinling–Dabie orogen, the North China Block to the north, the South China Block to the east, and the Qiangtang Block to the south (e.g., Bruguier et al., 1997; Nie et al., 1994; She et al., 2006; Weislogel, 2008; Weislogel et al., 2006; Zhang et al., 2006b; Zhou and Graham, 1996). This also implies that, although the Triassic sedimentary rocks in the eastern Songpan–Ganzi basin belonged to deposits of a possible foreland basin (Yuan et al., 2010), contemporaneous rocks in the central-western Songpan–Ganzi basin represent deposits in a remnant ocean basin (Yin and Harrison, 2000). Yin and Harrison (2000) also suggested that there was a relatively small forearc basin south of the Anyimaqen–Kunlun–Muztagh suture. Xiao et al. (2005) further suggested that the Late Triassic–Late Jurassic collision between the southern Kunlun and Northern Qiangtang active margins possibly generated a collisional complex including two forearc basins and their accretionary complexes. This kind of collision is typical in accretionary orogens, which can be found in modern examples like the Molucca Sea (Hall, 2002) and their ancient counterparts such as Inner Mongolia (Xiao et al., 2003), the Kelameili suture between the Northern Tianshan arcs and the East Junggar arcs (Xiao et al., 2004), and the Mongol–Okhotsk suture (Tomurtogoo et al., 2005). Therefore, we suggest that the northern Hohxil high-Mg andesites and dacite suites, occurring just south of the Anyimaqen–Kunlun–Muztagh suture, were most likely generated in a forearc setting (Fig. 10), which is similar to those of some high-Mg andesites in Cenozoic arcs (Tatsumi and Maruyama, 1989).

7. Conclusions

The northern Hohxil high-Mg andesites are dated by U-Pb zircon at 211 ± 2 Ma, and the dacites are dated by $^{40}Ar/^{39}Ar$ at 210.4 ± 1.9 Ma. The high-Mg andesites are geochemically similar to sanukitoids from the Cenozoic arc of southeastern Japan. Their augites exhibit compositional zoning marked by higher FeO, Na_2O and Al_2O_3 but lower $Mg^{\#}$ and CaO values in the cores than in the rims. The dacites have major and trace element characteristics similar to those of slab-derived adakites in modern arc systems. Both high-Mg andesites and dacites exhibit strongly fractionated platinum group element patterns coupled with uniformly low $\varepsilon Nd(t)$ values and high $(^{86}Sr/^{87}Sr)_i$ ratios. The Hohxil dacites were most probably produced by partial melting of subducted sediments above the northward-dipping central-western Songpan–Ganzi oceanic slab, and the high-Mg andesites were formed by the interaction between the sediment-derived melts and mantle peridotites. The Triassic Songpan–Ganzi basin is therefore implied to have experienced a double-sided subduction that lasted until, and eventually led to, its final closure in the Late Triassic. This interpretation, which links the tectonic evolution of the Kunlun–Qaidam Block in the north with that of the Qiangtang Block in the south, is consistent with the Triassic remnant ocean model that accounts for the origin of the central-western part of the Songpan–Ganzi basin.
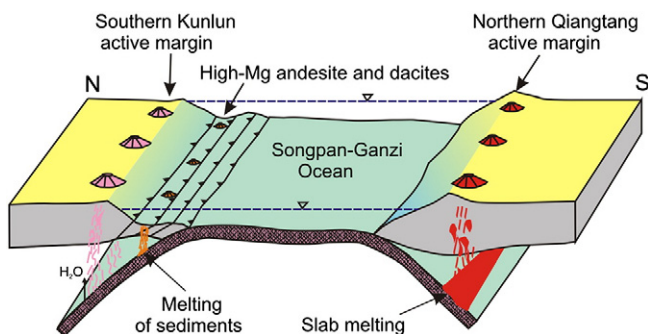
Fig. 10. A suggested model for Triassic tectonic evolution and magmatism in the vicinity of the central-western Hohxil–Songpan–Ganzi Block (modified from Xiao et al. (2002a, b) and Yin and Harrison (2000).

Appendix A. Supplementary data

Supplementary data to this article can be found online at doi:10.1016/j.lithos.2011.06.002.

References

Andersen, T., 2002. Correction of common lead in U–Pb analyses that do not report ^{204}Pb. Chemical Geology 192, 59–79.

Arculus, R.J., 2003. Use and abuse of the terms calcalkaline and calcalkalic. Journal of Petrology 44, 929–935.

Barnes, S.J., Boyd, R., Korneliusson, A., Nilsson, L.P., Often, M., Pedersen, R.B., Robins, B., 1988. The use of mantle normalization and metal ratios in discriminating between the effects of partial melting, crystal fractionation and sulphide segregation on platinum-group elements, gold, nickel and copper: examples from Norway. In: Prichard, H.M., Potts, P.J., Bowles, J.F.W., Cribb, S.J. (Eds.), Geo-platinum 87. Elsevier, London, pp. 113–143.

Boynton, W.V., 1984. Cosmochemistry of the earth elements: meteorite studies. In: Henderson, R. (Ed.), Rare Earth Element Geochemistry. Developments in Geochemistry, Vol. 2. Elservier, Amsterdam, pp. 89–92.

Bruguier, O., Lancelot, J.R., Malavieille, J., 1997. U–Pb dating on single detrital zircon grains from the Triassic Songpan–Ganze flysch (Central China): provenance and tectonic correlations. Earth and Planetary Science Letters 152, 217–231.

Burchfiel, B.C., Chen, Z., Liu, Y., Royden, L.H., 1995. Tectonics of the Longmen Shan and adjacent regions, central China. International Geology Review 37, 661–735.

Calmus, T., Aguillon-Robles, A., Maury, R.C., Bellon, H., Benoit, M., Cotten, J., Bourgois, J., Michaud, F., 2003. Spatial and temporal evolution of basalts and magnesian andesites ("bajaites") from Baja California, Mexico: the role of slab melts. Lithos 66 (1–2), 77–105.

Castillo, P.R., Janney, P.E., Solidum, R.U., 1999. Petrology and geochemistry of Camiguin island, southern Philippines: insights to the source of adakites and other lavas in a complex arc setting. Contributions to Mineralogy and Petrology 134, 33–51.

Chung, S.L., Chu, M.F., Zhang, Y., Xie, Y., Lo, C.H., Lee, T.Y., Lan, C.Y., Li, X., Zhang, Q., Wang, Y., 2005. Tibetan tectonic evolution inferred from spatial and temporal variations in post-collisional magmatism. Earth-Science Reviews 68 (3–4), 173–196.

Chung, S.L., Jahn, B.M., 1995. Plume-lithosphere interaction in generation of the Emeishan flood basalts at the Permian–Triassic boundary. Geology 23, 889–892.

Condie, K.C., 2003. Incompatible element ratios in oceanic basalts and komatiites: tracking deep mantle sources and continental growth rates with time. Geochemistry Geophysics Geosystems 4 (1), 1005. doi:10.1029/2002GC000333.

Defant, M.J., Drummond, M.S., 1990. Derivation of some modern arc magmas by melting of young subducted lithosphere. Nature 347, 662–665.

Drummond, M.S., Defant, M.J., 1990. A model for trondhjemite–tonalite–dacite genesis and crustal growth via slab melting: Archean to modern composition. Journal of Geophysical Research 95, 21503–21521.

Fu, X.G., Wang, J., Tan, F.W., Chen, M., Chen, W.B., 2010. The Late Triassic rift-related volcanic rocks from eastern Qiangtang, northern Tibet (China): age and tectonic implications. Gondwana Research 17 (1), 135–144.

Gao, S., Rudnick, R.L., Yuan, H.L., Liu, X.M., Liu, Y.S., Xu, W.L., Ling, W.L., Ayers, J., Wang, X.C., Wang, Q.H., 2004. Recycling lower continental crust in the North China Craton. Nature 432 (7019), 892–897.

Hall, R., 2002. Cenozoic geological and plate tectonic evolution of SE Asia and the SW Pacific: computer-based reconstructions, model and animations. Journal of Asian Earth Sciences 20 (4), 353–431.

Harris, N.B.W., Xu, R., Lewis, C.L., Hawkesworth, C.J., Zhang, Y., 1988. Isotope geochemistry of the 1985 Tibet Geotraverse, Lhasa to Golmud. Philosophical Transactions of the Royal Society of London, series A 327, 263–285.

Huang, M.H., Buick, I.S., Hou, L.W., 2003. Tectonometamorphic evolution of the eastern Tibet Plateau: evidence from the Central Songpan–Garze Orogenic Belt, Western China. Journal of Petrology 44 (2), 255–278.

Huang, X.L., Xu, Y.G., Lo, C.H., Wang, R.C., Lin, C.Y., 2007. Exsolution lamellae in a clinopyroxene megacryst aggregate from Cenozoic basalt, Leizhou Peninsula, South China: petrography and chemical evolution. Contributions to Mineralogy and Petrology 154, 691–705.

Johnson, M.C., Plank, T., 1999. Dehydration and melting experiments constrain the fate of subducted sediments. Geochemistry Geophysics Geosystems 1 1999GC000014.

Kapp, P., Yin, A., Manning, C.E., Harrison, T.M., Taylor, M.H., Ding, L., 2003. Tectonic evolution of the early Mesozoic blueschist-bearing Qiangtang metamorphic belt, central Tibet. Tectonics 22, 1043. doi:10.1029/2002TC001383.

Kay, S.M., Ramos, V.A., Marquez, M., 1993. Evidence in Cerro Pampa volcanic rocks for slab-melting prior to ridge–trench collision in southern South America. The Journal of Geology 101, 703–714.

Kelemen, P.B., Rilling, J.L., Parmentier, E.M., Mehl, L., Hacker, B.R., 2003. Thermal structure due to solid-state flow in the mantle wedge beneath arcs. Inside the Subduction Factory, Geophysical Monograph 138, 293–311.

Kepezhinskas, P., Defant, M.J., Widom, E., 2002. Abundance and distribution of PGE and Au in the island-arc mantle: implications for sub-arc metasomatism. Lithos 60 (3–4), 113–128.

Koppers, A.A.P., 2002. ArArCALC — software for ^{40}Ar/^{39}Ar age calculations. Computers & Geosciences 28, 605–619.

Li, X.-H., Li, Z.-X., Zhou, H., Liu, Y., Kinny, P.D., 2002. U–Pb zircon geochronology, geochemistry and Nd isotopic study of Neoproterozoic bimodal volcanic rocks in the Kangdian Rift of South China: implications for the initial rifting of Rodinia. Precambrian Research 113 (1–2), 135–154.

Li, Z.X., Li, X.H., Kinny, P.D., Wang, J., Zhang, S., Zhou, H., 2003. Geochronology of Neoproterozoic syn-rift magmatism in the Yangtze Craton, South China and correlations with other continents: evidence for a mantle superplume that broke up Rodinia. Precambrian Research 122 (1–4), 85–109.

Liu, Y.S., Gao, S., Gao, C.G., Wang, D.B., Zong, K.Q., Hu, Z.C., 2010. Timing of melt-peridotite interactions in xenoliths of the Trans-North China Orogen: U–Pb dating, Hf isotopes and trace elements in zircon. Journal of Petrology 51 (1–2), 537–571.

Macpherson, C.G., Dreher, S.T., Thirlwall, M.F., 2006. Adakites without slab melting: high pressure differentiation of island arc magma, Mindanao, the Philippines. Earth and Planetary Science Letters 243 (3–4), 581–593.

McDonough, W.F., Sun, S.S., 1995. The composition of the Earth. Chemical Geology 120 (3–4), 223–253.

Nie, S., Yin, A., Rowley, D.B., Jin, Y., 1994. Exhumation of the Dabie Shan ultrahigh-pressure rocks and accumulation of the Songpan–Ganzi flysch sequence, central China. Geology 22, 999–1002.

Niu, Y., Batiza, R., 1997. Trace element evidence from seamounts for recycled oceanic crust in the eastern equatorial Pacific mantle. Earth and Planetary Science Letters 148, 471–484.

Peccerillo, A., Taylor, S.R., 1976. Geochemistry of Eocene calc-alkaline volcanic rocks from the Kastamonu area, Northern Turkey. Contributions to Mineralogy and Petrology 58 (1), 63–81.

Plank, T., 2005. Constraints from Thorium/Lanthanum on sediment recycling at subduction zones and the evolution of the continents. Journal of Petrology 46 (5), 921–944.

Plank, T., Langmuir, C.H., 1998. The chemical composition of subducting sediment and its consequences for the crust and mantle. Chemical Geology 145, 325–394.

Puchtel, I.S., Haase, K.M., Hofmann, A.W., Chauvel, C., Kulikov, V.S., Garbe-Schönberg, C.D., Nemchin, A.A., 1997. Petrology and geochemistry of crustally contaminated komatiitic basalts from the Vetreny Belt, southeastern Baltic Shield: evidence for an early Proterozoic mantle plume beneath rifted Archean continental lithosphere. Geochimica et Cosmochimica Acta 61, 1205–1222.

Pullen, A., Kapp, P., Gehrels, G.E., Vervoort, J.D., Ding, L., 2008. Triassic continental subduction in central Tibet and Mediterranean-style closure of the Paleo-Tethys Ocean. Geology 36 (5), 351–354.

Qinghai, B.G.M.R., 1991. (Qinghai Bureau of Geology and Mineral Resources). Regional Geology of Qinghai Province. Geological Publishing House, Beijing, p. 662.

Qiu, H.N., Jiang, Y.D., 2007. Sphalerite ^{40}Ar/^{39}Ar progressive crushing and stepwise heating techniques. Earth and Planetary Science Letters 256, 224–232.

Rapp, R.P., Shimizu, N., Norman, M.D., 2003. Growth of early continental crust by partial melting of eclogite. Nature 425, 605–609.

Rapp, R.P., Shimizu, N., Norman, M.D., Applegate, G.S., 1999. Reaction between slab-derived melts and peridotite in the mantle wedge: experimental constraints at 3.8 GPa. Chemical Geology 160 (4), 335–356.

Reid, A., Wilson, C.J.L., Shun, L., Pearson, N., Belousova, E., 2007. Mesozoic plutons of the Yidun Arc, SW China: U/Pb geochronology and Hf isotopic signature. Ore Geology Reviews 31 (1–4), 88–106.

Roger, F., Arnaud, N., Gilder, S., Tapponnier, P., Jolivet, M., Brunel, M., Malavieille, J., Xu, Z.Q., Yang, J.S., 2003. Geochronological and geochemical constraints on Mesozoic suturing in east central Tibet. Tectonics 22 (4), 1037. doi:10.1029/2002TC001466.

Roger, F., Calassou, S., 1997. U–Pb geochronology on zircon and isotopic geochemistry (Pb, Sr and Nd) of the basement in the Songpan–Garze fold belt (China). Comptes Rendus de l'Académie des Sciences – Series IIA – Earth and Planetary Science 324, 819–826.

Roger, F., Malavieille, J., Leloup, P.H., Calassou, S., Xu, Z., 2004. Timing of granite emplacement and cooling in the Songpan–Garz-Fold Belt (eastern Tibetan Plateau) with tectonic implications. Journal of Asian Earth Sciences 22 (5), 465–481.

Rudnick, R.L., Barth, M.G., Horn, I., McDonough, W.F., 2000. Rutile-bearing refractory eclogites: missing link between continents and depleted mantle. Science 287, 278–281.

Rudnick, R.L., Gao, S., 2003. Composition of the continental crust. In The Crust (ed. R. L. Rudnick) Vol. 3 Treatise on Geochemistry (eds. H. D. Holland and K. K. Turekian) [M]. Elsevier-Pergamon, Oxford (2003). P., 1–64.

Saunders, A.D., Rogers, G., Marriner, G.F., Terrell, D.J., Verma, S.P., 1987. Geochemistry of Cenozoic volcanic rocks, Baja California, Mexico: implications for the petrogenesis of post-subduction magmas. Journal of Volcanology and Geothermal Research 32, 223–245.

Schmidt, M.W., Vielzeuf, D., Auzanneau, E., 2004. Melting and dissolution of subducting crust at high pressures: the key role of white mica. Earth and Planetary Science Letters 228, 65–84.

Şengör, A.M.C., Altiner, D., Cin, A., Ustaömer, T., Hsü, K.J., 1988. Origin and assembly of the Tethyside orogenic collage at the expense of Gondwanaland, in Gondwana and Tethys, edited by Audley-Charles M. G. and Hallam A. Geological Society, London. Special Publications 37, 119–181.

Setiabudi, B.T., Campbell, I.H., Martin, C.E., Allen, C.M., 2007. Platinum group element geochemistry of andesite intrusions of the Kelian Region, East Kalimantan, Indonesia: implications of gold depletion in the intrusions associated with the Kelian Gold Deposit. Economic Geology 102 (1), 95–108.

She, Z., Ma, C., Mason, R., Li, J., Wang, G., Lei, Y., 2006. Provenance of the Triassic Songpan–Ganzi flysch, west China. Chemical Geology 231 (1–2), 159–175.

Shimoda, G., Tatsumi, Y., Nohda, S., Ishizaka, K., Jahn, B.M., 1998. Setouchi high-Mg andesites revisited: geochemical evidence for melting of subducting sediments. Earth and Planetary Science Letters 160 (3–4), 479–492.

Song, X.-Y., Zhou, M.-F., Cao, Z.-M., Robinson, P.T., 2004. Late Permian rifting of the South China Craton caused by the Emeishan mantle plume? Journal of the Geological Society. London 161 (5), 773–781.

Streck, M.J., Leeman, W.P., Chesley, J., 2007. High-magnesian andesite from Mount Shasta: a product of magma mixing and contamination, not a primitive mantle melt. Geology 35 (4), 351–354.

Sun, S.S., McDonough, W.F., 1989. Chemical and isotopic systematics of oceanic basalts: implications for mantle composition and processes. In Saunders, A. D. and Norry, M. J. (eds.), Implications for Mantle Composition and Processes, Magmatism in the Ocean Basins. Geological Society, London. Special Publications 42, 313–345.

Sun, Y., Sun, M., 2005. Nickel sulfide fire assay improved for pre-concentration of platinum group elements in geological samples: a practical means of ultra-trace analysis combined with inductively coupled plasma-mass spectrometry. The Analyst 130, 664–669.

Tatsumi, Y., 2001. Geochemical modeling of partial melting of subducting sediments and subsequent melt-mantle interaction: generation of high-Mg andesites in the Setouchi volcanic belt, southwest Japan. Geology 29 (4), 323–326.

Tatsumi, Y., Hanyu, T., 2003. Geochemical modeling of dehydration and partial melting of subducting lithosphere: toward a comprehensive understanding of high-Mg andesite formation in the Setouchi volcanic belt, SW Japan. Geochemistry Geophysics Geosystems 4, 1081. doi:10.1029/2003GC000530.

Tatsumi, Y., Ishizaka, K., 1981. Existence of andesitic primary magma: an example from southwest Japan. Earth and Planetary Science Letters 53, 124–130.

Tatsumi, Y., Maruyama, S., 1989. Boninites and high-Mg andesites: tectonics and petrogenesis. In: Crawford, A. (Ed.), Boninites and Related Rocks. Unwin Hyaman, pp. 50–71.

Taylor, R.N., Nesbitt, R.W., Vidal, P., Harmon, R.S., Auvray, B., Croudace, I.W., 1994. Mineralogy, chemistry, and genesis of the boninite series volcanics, Chichijima, Bonin-Islands, Japan. Journal of Petrology 35 (3), 577–617.

Tomurtogoo, O., Windley, B.F., Kroner, A., Badarch, G., Liu, D.Y., 2005. Zircon age and occurrence of the Adaatsag ophiolite and Muron shear zone, central Mongolia: constraints on the evolution of the Mongol–Okhotsk ocean, suture and orogen. Journal of the Geological Society, London 162 (1), 125–134.

Umino, S., 1986. Magma mixing in boninite sequence of Chichijima, Bonin Islands. Journal of Volcanology and Geothermal Research 29 (1–4), 125–157.

Wang, J., Fu, X.G., Chen, W.X., Wang, Z.J., Tan, F.W., Chen, M., Zhuo, J.W., 2008a. Chronology and geochemistry of the volcanic rocks in Woruo mountain region, northern Qiangtang depression: implications to the Late Triassic volcanic–sedimentary events. Science in China Series D-Earth Sciences 51, 194–205.

Wang, Q., Wyman, A., Xu, J.F., Wan, Y.S., Li, C.F., Zi, F., Jiang, Z.Q., Qiu, H.N., Chu, Z.Y., Zhao, Z.H., Dong, Y.H., 2008b. Triassic Nb-enriched basalts, magnesian andesites, and adakites of the Qiangtang terrane (Central Tibet): evidence for metasomatism by slab-derived melts in the mantle wedge. Contributions to Mineralogy and Petrology 155, 73–490.

Wang, Q., Wyman, D.A., Xu, J.F., Dong, Y.H., Vasconcelos, P.M., Pearson, N., Wan, Y., Dong, H., Li, C.F., Yu, Y.S., Zhu, T.X., Feng, X.T., Zhang, Q.Y., Zi, F., Chu, Z.Y., 2008c. Eocene melting of subducting continental crust and early uplifting of central Tibet: evidence from central-western Qiangtang high-K calc-alkaline andesites, dacites and rhyolites. Earth and Planetary Science Letters 272 (1–2), 158–171.

Wang, Q., Wyman, D.A., Xu, J.F., Zhao, Z.H., Jian, P., Xiong, X.L., Bao, Z.W., Li, C.F., Bai, Z.H., 2006a. Petrogenesis of Cretaceous adakitic and shoshonitic igneous rocks in the Luzong area, Anhui Province (eastern China): implications for geodynamics and Cu–Au mineralization. Lithos 89 (3–4), 424–446.

Wang, Q., Wyman, D.A., Zhao, Z.-H., Xu, J.-F., Bai, Z.-H., Xiong, X.-L., Dai, T.-M., Li, C.-F., Chu, Z.-Y., 2007. Petrogenesis of Carboniferous adakites and Nb-enriched arc basalts in the Alataw area, northern Tianshan Range (western China): implications for Phanerozoic crustal growth in the Central Asia orogenic belt. Chemical Geology 236 (1–2), 42–64.

Wang, Q., Xu, J.F., Jian, P., Bao, Z.W., Zhao, Z.H., Li, C.F., Xiong, X.L., Ma, J.L., 2006b. Petrogenesis of adakitic porphyries in an extensional tectonic setting, Dexing, South China: implications for the genesis of porphyry copper mineralization. Journal of Petrology 47 (1), 119–144.

Watson, M.P., Hayward, A.B., Parkinson, D.N., Zhang, Z.M., 1987. Plate tectonic history, basin development and petroleum source rock deposition onshore China. Marine and Petroleum Geology 4 (3), 205–225.

Weislogel, A.L., 2008. Tectonostratigraphic and geochronologic constraints on evolution of the northeast Paleotethys from the Songpan–Ganzi complex, central China. Tectonophysics 451 (1–4), 331–345.

Weislogel, A.L., Graham, S.A., Chang, E.Z., Wooden, J.L., Gehrels, G.E., Yang, H., 2006. Detrital zircon provenance of the Late Triassic Songpan–Ganzi complex: sedimentary record of collision of the North and South China Blocks. Geology 34, 97–100.

Wilson, C.J.L., Harrowfield, M.J., Reid, A.J., 2006. Brittle modification of Triassic architecture in eastern Tibet: implications for the construction of the Cenozoic plateau. Journal of Asian Earth Sciences 27 (3), 341–357.

Winchester, J.A., Floyd, P.A., 1977. Geochemical discrimination of different magma series and their differentiation products using immobile elements. Chemical Geology 20, 325–343.

Wittlinger, G., Masson, F., Poupinet, G., Tapponnier, P., Mei, J., Herquel, G., Guilbert, J., Achaire, U., Guanqi, X., Danian, S., Lithoscope Kunlun, T., 1996. Seismic tomography of northern Tibet and Kunlun: evidence for crustal blocks and mantle velocity contrasts. Earth and Planetary Science Letters 139 (1–2), 263–279.

Xiao, L., Xu, J.F., 2005. Petrogenesis and tectonic setting of Dashibao Group basalts from Songpan–Ganze Block, northwestern Sichuan province, China. Acta Geologica Sinica 21, 1539–1545.

Xiao, L., Zhang, H.F., Clemens, J.D., Wang, Q.W., Kan, Z.Z., Wang, K.M., Ni, P.Z., Liu, X.M., 2007. Late Triassic granitoids of the eastern margin of the Tibetan Plateau: geochronology, petrogenesis and implications for tectonic evolution. Lithos 96, 436–452.

Xiao, W.J., Windley, B., Hao, J.I.E., Li, J., 2002a. Arc-ophiolite obduction in the Western Kunlun Range (China): implications for the Palaeozoic evolution of central Asia. The Journal of Geology Society, London 159 (5), 517–528.

Xiao, W.J., Windley, B.F., Chen, H.L., Zhang, G.C., Li, J.L., 2002b. Carboniferous-Triassic subduction and accretion in the western Kunlun, China: implications for the collisional and accretionary tectonics of the northern Tibetan plateau. Geology 30, 295–298.

Xiao, W.J., Windley, B.F., Liu, D.Y., Jian, P., Liu, C.Z., 2005. Paleozoic accretionary tectonics of the Western Kunlun Range, China: new SHRIMP zircon ages from the Kudi ophiolite and associated granites, and implications for the crustal growth of Central Asia. Journal of Geology 113, 687–705.

Xiao, W.J., Windley, B.F., Hao, J., Zhai, M.G., 2003. Accretion leading to collision and the Permian Solonker suture, Inner Mongolia, China: termination of the central Asian orogenic belt. Tectonics 22 (6), 1069. doi:10.1029/2002TC001484.

Xiao, W.-J., Zhang, L.-C., Qin, K.-Z., Sun, S., Li, J.-L., 2004. Paleozoic accretionary and collisional tectonics of the Eastern Tianshan (China): implications for the continental growth of central Asia. American Journal of Science 304, 370–395.

Xiong, X.L., Adam, J., Green, T.H., 2005. Rutile stability and rutile/melt HFSE partitioning during partial melting of hydrous basalt: implications for TTG genesis. Chemical Geology 218, 339–359.

Xu, W., Hergt, J.M., Gao, S., Pei, F., Wang, W., Yang, D., 2008. Interaction of adakitic melt-peridotite: implications for the high-Mg$^{\#}$ signature of Mesozoic adakitic rocks in the eastern North China Craton. Earth and Planetary Science Letters 265 (1–2), 123–137.

Yin, A., Harrison, T.M., 2000. Geologic evolution of the Himalayan–Tibetan orogen. Annual Review of Earth and Planetary Sciences 28, 211–280.

Yogodzinski, G.M., Kay, R.W., Volynets, O.N., Koloskov, A.V., Kay, S.M., 1995. Magnesian andesite in the western Aleutian Komandorsky region — implications for slab melting and processes in the mantle wedge. Geological Society of American Bulletin 107 (5), 505–519.

Yogodzinski, G.M., Kelemen, P.B., 1998. Slab melting in the Aleutians: implications of an ion probe study of clinopyroxene in primitive adakite and basalt. Earth and Planetary Science Letters 158 (1–2), 53–65.

Yogodzinski, G.M., Lees, J.M., Churikova, T.G., Doreneorf, F., Woerner, G., Volynets, O.N., 2001. Geochemical evidence for the melting of subducting oceanic lithosphere at plate edges. Nature 409, 500–504.

Yogodzinski, G.M., Volynets, O.N., Koloskov, A.V., Seliverstov, N.I., Matvenkov, V.V., 1994. Magnesian andesites and the subduction component in a strongly calc-alkaline series at Piip Volcano, far western Aleutians. Journal of Petrology 35 (1), 163–204.

Yuan, C., Sun, M., Xiao, W.J., Wilde, S., Li, X.H., Liu, X.H., Long, X.P., Xia, X.P., Ye, K., Li, J.L., 2009. Garnet-bearing tonalitic porphyry from East Kunlun, Northeast Tibetan Plateau: implications for adakite and magmas from the MASH Zone. International Journal of Earth Sciences 98, 1489–1510.

Yuan, C., Zhou, M.-F., Sun, M., Zhao, Y., Wilde, S., Long, X., Yan, D., 2010. Triassic granitoids in the eastern Songpan Ganzi Fold Belt, SW China: magmatic response to geodynamics of the deep lithosphere. Earth and Planetary Science Letters 290 (3–4), 481–492.

Zhang, H.-F., Parrish, R., Zhang, L., Xu, W.-C., Yuan, H.-L., Gao, S., Crowley, Q.G., 2007a. A-type granite and adakitic magmatism association in Songpan–Garze fold belt, eastern Tibetan Plateau: implication for lithospheric delamination. Lithos 97 (3–4), 323–335.

Zhang, H.F., Sun, M., Zhou, X.H., Fan, W.M., Zhai, M.G., Yin, J.F., 2002. Mesozoic lithosphere destruction beneath the North China Craton: evidence from major-, trace- element and Sr–Nd–Pb isotope studies of Fangcheng basalts. Contributions to Mineralogy and Petrology 144, 241–253.

Zhang, H.F., Xu, W.C., Guo, J.Q., Zong, K.Q., Cai, H.M., Yuan, H.L., 2007b. Indosinian orogenesis of the Gangdise Terrane:evidences from zircon U-Pb dating and petrogenesis of granitoids. Earth Science-Journal of China University of Geosciences 32, 155–166 (in Chinese with English abstract).

Zhang, H.F., Zhang, L., Harris, N., Jin, L.L., Yuan, H.L., 2006a. U–Pb zircon ages, geochemical and isotopic compositions of granitoids in Songpan–Garze fold belt, eastern Tibetan Plateau: constraints on petrogenesis and tectonic evolution of the basement. Contributions to Mineralogy and Petrology 152, 75–88.

Zhang, K.J., Cai, J.X., Zhang, Y.X., Zhao, T.P., 2006b. Eclogites from central Qiangtang, northern Tibet (China) and tectonic implications. Earth and Planetary Science Letters 245 (3–4), 722–729.

Zhou, D., Graham, S.A., 1996. Songpan–Ganzi Triassic flysch complex of the West Qinling Shan as a remnant ocean basin. In: Yin, A., Harrison, M. (Eds.), The Tectonic Evolution of Asia. Cambridge University Press, Cambridge, pp. 281–299.

Zhou, J., 1999. Geochemistry and Petrogenesis of Igneous Rocks Containing Amphibole and Mica: a Case Study of Plate Collision Involving Scotland and Himalayas. Science Press New York, Beijing. p. 41–72.

Zhu, Y.T., Guo, T.Z., Zhang, X.T., Yang, Y.X., Peng, C., Peng, W., 2003. Discovery of Triassic Norian strata in the Hoh Xil Lake area, western Qinghai, and its geological significance. Geological Bulletin of China 22, 474–479.